

# 1 Cluster-based characterization of multi-dimensional tropospheric 2 ozone variability in coastal regions: an analysis of lidar 3 measurements and model results

4 Claudia Bernier<sup>1</sup>, Yuxuan Wang<sup>1</sup>, Guillaume Gronoff<sup>2,3</sup>, Timothy Berkoff<sup>2</sup>, K. Emma Knowland<sup>4,5</sup>, John T.  
5 Sullivan<sup>4</sup>, Ruben Delgado<sup>6,7</sup>, Vanessa Caicedo<sup>6,7</sup>, Brian Carroll<sup>2,6</sup>

6 <sup>1</sup>Department of Earth and Atmospheric Science, University of Houston, Houston, Texas, USA

7 <sup>2</sup>NASA Langley Research Center, Hampton, VA, 23666, USA

8 <sup>3</sup>Science Systems and Application Inc., Hampton, VA, 23666, USA

9 <sup>4</sup>NASA Goddard Space Flight Center, Global Modeling and Assimilation Office, Greenbelt, MD, 20771, USA

10 <sup>5</sup>Morgan State University, Goddard Earth Science Technology & Research (GESTAR) II, Baltimore, Maryland, USA

11 <sup>6</sup>Joint Center for Earth Systems Technology, Baltimore, MD, USA

12 <sup>7</sup>University of Maryland Baltimore County, Baltimore, MD, USA

13 *Correspondence:* Yuxuan Wang (ywang246@central.uh.edu)

14

15 **Abstract.** Coastal regions are susceptible to multiple complex dynamic and chemical mechanisms and emission sources that  
16 lead to frequently observed large tropospheric ozone variations. These large ozone variations occur on a meso-scale which  
17 have proven to be arduous to simulate using chemical transport models (CTMs). We present a clustering analysis of multi-  
18 dimensional measurements from ozone Light Detection And Ranging (LiDAR) in conjunction with both an offline GEOS-  
19 Chem CTM simulation and the online GEOS-Chem simulation GEOS-CF, to investigate the vertical and temporal variability  
20 of coastal ozone during three recent air quality campaigns: 2017 Ozone Water-Land Environmental Transition Study  
21 (OWLETS)-1, 2018 OWLETS-2, and 2018 Long Island Sound Tropospheric Ozone Study (LISTOS). We developed and  
22 tested a clustering method that resulted in 5 ozone profile curtain clusters. The established 5 clusters all varied significantly in  
23 ozone magnitude vertically and temporally which allowed us to characterize the coastal ozone behavior. The lidar clusters  
24 provided a simplified way to evaluate the two CTMs for their performance of diverse coastal ozone cases. An overall evaluation  
25 of the models reveals good agreement ( $R \approx 0.70$ ) in the low-level altitude range (0 to 2000 m), with a low and unsystematic  
26 bias for GEOS-Chem and high systemic positive bias for GEOS-CF. The mid-level (2000 – 4000 m) performances show a  
27 high systematic negative bias for GEOS-Chem and an overall low unsystematic bias for GEOS-CF and a generally weak  
28 agreement to the lidar observations ( $R = 0.12$  and  $0.22$ , respectively). ~~In eEvaluating the cluster-by-cluster cluster-specific~~  
29 ~~model performances additional model insight is reveals additional model insight that is overlooked in the overall model~~  
30 ~~performance.ed as cluster by cluster model performance is more convoluted than the overall performances suggest.~~ Utilizing

31 the full vertical and diurnal ozone distribution information specific to lidar measurements, this work provides new insights on  
32 model's proficiency in complex coastal regions.

33

## 34 1. Introduction

35 Tropospheric ozone ( $O_3$ ) is an important secondary pollutant created by multiple reactions involving sunlight, nitrogen  
36 oxides ( $NO_x = NO + NO_2$ ), and volatile organic compounds (VOCs) which, in accumulation, can have damaging effects on  
37 human and plant health. In addition to its photochemical growth,  $O_3$  can easily be influenced by local and regional transport  
38 mechanisms. For coastal regions, surface  $O_3$  is highly variable in time and space due to its susceptibility to many factors such  
39 as local ship emissions, long range transport, and sea/bay breeze processes. ~~Multiple studies have proven the strong influence  
40 that sea/bay breeze and wind flow patterns can have on the accumulation of coastal  $O_3$  and can often lead to poor air quality  
41 (e.g., Tucker et al., 2010; Martins et al., 2012; Stauffer et al., 2012; Li et al., 2020). Loughner et al. (2014) also highlighted the  
42 importance of understanding the ability for bay breeze events to cause  $O_3$  variability not only spatially but vertically in coastal  
43 regions.~~

44 This variability is challenging for air quality models to capture as high-resolution measurements are necessary to fully  
45 understand and simulate this  $O_3$  behavior in coastal regions.

46 For example, Dreessen et al. (2019) tested the U.S. Environmental Protection Agency (EPA) Community Multiscale Air  
47 Quality (CMAQ) model's ability, configured at 12 km, to simulate  $O_3$  exceedances at Hart Miller Island in Maryland (HMI)  
48 revealing high bias and 'false alarms' due to several reasons such as emission transport over water and the coarse model  
49 resolution's inability to capture fine-scale meteorology and transport. ~~Multiple studies have proven the strong influence that  
50 sea/bay breeze and wind flow patterns can have on the accumulation of coastal  $O_3$  and can often lead to poor air quality (e.g.,  
51 Tucker et al., 2010; Martins et al., 2012; Stauffer et al., 2012; Li et al., 2020).~~ Cases such as sea/bay breeze events, which  
52 directly contribute to high coastal  $O_3$  cases, are denoted by local meteorological mechanisms such as surface wind speed  
53 deceleration, wind direction convergence and recirculation (Banta et al., 2005). ~~Loughner et al. (2014) also highlighted the  
54 importance of understanding the ability bay breeze events have in  $O_3$  variability not only spatially but vertically throughout  
55 the atmosphere.~~ Air quality models with coarse horizontal and vertical resolutions are not able to capture such fine  
56 developments (Caicedo et al., 2019). Ring et al. (2018) also used CMAQ to estimate the impact of ship emissions on the air  
57 quality in eastern U.S. coastal regions indicating that an understanding of the vertical profiles of emissions was significant for  
58 improving air quality simulations. These are consistent and unanimous issues with air quality modeling in coastal regions.  
59 Since offshore sites within coastal regions are historically under sampled due to the difficulty of water-based measurements,  
60 this problem is still pertinent today.

61 Recently, three associated air quality campaigns set out to address this issue (<https://www-air.larc.nasa.gov/index.html>):  
62 2017 & 2018 NASA Ozone Water-Land Environmental Transition Study (OWLETS-1 & OWLETS-2) and Long Island Sound  
63 Tropospheric Ozone Study (LISTOS) (e.g., Sullivan et al., 2019). These three campaigns were each conducted in highly  
64 populated coastal regions along the Chesapeake Bay in Virginia and Maryland and the Long Island Sound in the New

65 England/Middle Atlantic region, that are vulnerable to O<sub>3</sub> exceedances with the goal of filling the measurement gaps in these  
66 regions. During these campaigns, a suite of detailed airborne and ground measurements were taken during the course of highly  
67 polluted summer months (end of May through August) to capture the variability of pollutants, including O<sub>3</sub> and its precursor  
68 species, and the distinct meteorological processes specific to land-water regions that affect them.

69 The three campaigns strategically placed multi-dimensional tropospheric O<sub>3</sub> lidar instruments on and offshore in order to  
70 capture critical land-water gradients and to fill the deficit of measurements in these under monitored areas. These  
71 measurements were supported as part of NASA's Tropospheric Ozone Lidar Network (TOLNet). Continuous profile  
72 measurements from O<sub>3</sub> lidars highlight important regional transport and temporal variations of O<sub>3</sub> in the lower and middle  
73 levels of the troposphere that are usually difficult to capture by most satellite-based remote-sensing instruments (Thompson et  
74 al., 2014). Lidar instruments are unique in their ability to capture high resolution full O<sub>3</sub> 2-D profile curtains over a period of  
75 time that ~~indicate pollutant transport and~~ can help in understanding O<sub>3</sub> behavior in coastal regions. In Gronoff et al. (2019),  
76 the co-located lidar at the Chesapeake Bay Tunnel Bridge (CBBT) during OWLETS-1 successfully captured a near-surface  
77 maritime ship plume emission event on ~~August 01~~ August 7, 2017. An ensemble of other instruments (e.g., drones, Pandora  
78 spectrometer systems, etc.) launched near the shipping channel captured elevated NO<sub>2</sub> concentrations while the lidar  
79 instrument captured a depletion of O<sub>3</sub> simultaneously. The lidar was able to capture the unique low range altitude O<sub>3</sub>  
80 concentrations which elucidated the evolution of the trace-gas concentrations during this ship plume event.

81 Several studies have thoroughly evaluated the results from the air quality campaigns used in this study but were focused  
82 more on specific case studies (Dacic et al., 2019; Sullivan et al., 2019; Gronoff et al., 2019). Dacic et al. (2019) used lidar  
83 measurements of a high O<sub>3</sub> episode during OWLETS-1 to evaluate the ability of two NASA coupled chemistry-meteorology  
84 models (CCMMs), the GEOS Composition Forecast ("GEOS-CF"; Keller et al., 2021) and MERRA2-GMI (Strode et al.,  
85 2019), to simulate this high O<sub>3</sub> event. They found that the GEOS-CF model performed fairly in simulating O<sub>3</sub> in the lower  
86 level (between 400 to 2000 m ASL) and outperformed MERRA2-GMI based on surface observations at multiple monitoring  
87 sites ~~and by a median difference of 6 to 8 % +/- 7 % at both lidar sites~~. In the case of this event, GEOS-CF was able to simulate  
88 the 2-D O<sub>3</sub> profile curtains at small scales. At the time of the Dacic et al. (2019) study, ~~only~~ processed observational data was  
89 only available from OWLETS-1 ~~was available~~.

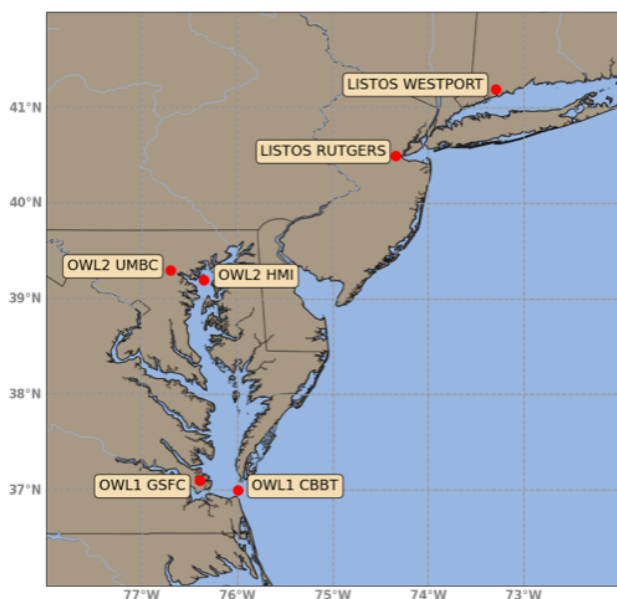
90 For this study, we took advantage of ~~91~~ measured 2-D (vertical and diurnal) O<sub>3</sub> profile curtains from all three air quality  
91 campaigns (Sect. 2). To characterize the different behaviors of O<sub>3</sub> in coastal regions, we developed a novel clustering method  
92 based on the altitude and time dimensions of the lidar measurements that organized the profile curtains (Sect. 2). We used the  
93 developed clusters to evaluate the ability of both offline and online GEOS-Chem and GEOS-CF simulations to reproduce the  
94 coastal O<sub>3</sub> and wind characteristics highlighted by each cluster (Sect. 3).

95

## 96 **2. Materials & Method**

### 97 **2.1. Air quality campaigns**

98 During the years 2017 and 2018, NASA in partnership with other U.S. national agencies and university research groups  
99 orchestrated three air quality campaign studies that focused on key land and water observations: OWLETS-1, OWLETS-2,  
100 and LISTOS. OWLETS-1 was conducted in 2017 from July 5 to August 3, while OWLETS-2 and LISTOS were conducted in  
101 2018 from June 6 to July 6 and July 12 to August 29, respectively. All campaigns took advantage of a multitude of ground,  
102 aircraft, and remote sensing measurements. For the sake of this study, we will focus on measurements from the two lidars from  
103 the TOLNet: NASA Langley Mobile Ozone Lidar (LMOL) (De Young et al. 2017; Farris et al. 2018; Gronoff et al, 2019,  
104 2021) and NASA Goddard Space Flight Center (GSFC) Tropospheric Ozone (TROPOZ) Differential Absorption Lidar (DIAL)  
105 (Sullivan et al. 2014, 2015a), which ran simultaneously at the marked positions in Figure 1. The TOLNet data from all three  
106 campaigns are available on the NASA LaRC Airborne Science Data for Atmospheric Composition archive ([https://www-  
107 air.larc.nasa.gov/missions.htm](https://www-air.larc.nasa.gov/missions.htm); accessed – 20 January 2021).  
108



109 **Figure 1.** An inset map of the Chesapeake Bay airshed in Maryland, Virginia, and Long Island Sound in New York with the  
110 six lidar monitoring locations used for OWLETS-1, OWLETS-2, and LISTOS highlighted and labeled.

111 The two lidars were placed strategically for each campaign (Figure 1), so that one lidar was closest to over-water  
112 measurements while the other was farther inland with the goal of examining how  $O_3$  transport and concentration is influenced  
113 by specific coastal mechanisms such as the land–water breezes. For OWLETS-1, the LMOL lidar was used at the CBBT  
114 [37.0366°N, 76.0767°W], depicting the real time over water  $O_3$  measurements while the GSFC TROPOZ lidar was stationed  
115 at NASA Langley Center [37.1024°N, 76.3929°W] further inland. Similarly, for OWLETS-2, the LMOL lidar was stationed  
116 for the over water measurements at Hart Miller Island [39.2449° N, 76.3583° W] and GSFC TROPOZ was stationed at the

117 University of Maryland, Baltimore County (UMBC) [39.2557° N, 76.7111° W]. ~~Finally, F~~ for LISTOS, LMOL was at the  
118 Westport site [41.1415° N, 73.3579° W] and TROPOZ at Rutgers [40.2823° N, 74.2525° W]. For the sake of this study the  
119 unique benefits due to the different placements (onshore versus offshore) of the co-located lidars are not specifically evaluated.  
120 Instead, the study focuses on the benefits of the detailed and multi-dimensionality of lidar instrument data in general.

121  
122 Routine lidar measurements were taken for the duration of the campaigns ~~providing 91 multi-dimensional O<sub>3</sub> profile~~  
123 ~~curtains~~. Both lidars retrieve data at a 5-min temporal resolution and use a common processing scheme to produce a final O<sub>3</sub>  
124 product which was used for this study. In this study, the individual profile curtains refer to the “full day”, vertical and diurnal  
125 lidar measurements. In this study, 91 individual 2-D profile curtains were used from both lidars from the three campaigns: 26  
126 profile curtains from OWLETS-1, 28 profile curtains from OWLETS-2, and 37 profile curtains from LISTOS.

127 To evaluate meteorological impacts on the lidar O<sub>3</sub> clusters and model performance we used various temperature and  
128 wind measurements. Hourly observed temperature, wind speed and wind direction, and O<sub>3</sub> from surface monitors pertaining  
129 to the study area were obtained from the Air Quality System (AQS) (data can be accessed at  
130 <https://aqs.epa.gov/aqsweb/airdata/>). We utilized high resolution vertical and horizontal wind speed and direction data  
131 monitored by Doppler wind lidar Leosphere WINDCUBE 200s instruments deployed at HMI during OWLETS-2 during  
132 LISTOS (e.g., Couillard et al., 2021; Coggon et al., 2021; Wu et al., 2021).

133

## 134 2.2. Clustering lidar data

### 135 2.2.1 Description of the ozone lidar measurements

136 The lidar instrument is unique in that it provides high dimensional profile measurements of O<sub>3</sub>, as opposed to one  
137 dimensional surface measurements from air quality monitoring sites. The two TOLNet lidars used during the campaigns have  
138 been evaluated for their accuracy during previous air quality campaigns (DISCOVER-AQ; [https://www-](https://www-air.larc.nasa.gov/missions/discover-aq)  
139 [air.larc.nasa.gov/missions/discover-aq](https://www-air.larc.nasa.gov/missions/discover-aq) and FRAPPÉ; <https://www2.acom.ucar.edu/frappe>) and have also been compared  
140 against each other (e.g., Sullivan et al., 2015; Wang et al., 2017). The two lidars have different transmitter and retrieval  
141 components but produce O<sub>3</sub> profiles within 10 % of each other as well as compared to ozonesondes (Sullivan et al., 2015). In  
142 comparison with other in situ instrument measurements, the TOLNet lidars were found to have an accuracy better than ±15 %  
143 for capturing high temporal tropospheric O<sub>3</sub> vertically proving their capability of capturing high temporal tropospheric O<sub>3</sub>  
144 variability (Wang et al., 2017; Leblanc et al., 2018).

145 To characterize coastal O<sub>3</sub> during the summer months, we use a multitude of lidar profile curtains obtained during the  
146 OWLETS-1, 2, and LISTOS campaigns. The two lidars used in the campaigns produced O<sub>3</sub> profile curtains from 0 – 6000 m  
147 above ground level (AGL) with some days beginning as early as 06:00 local time (EDT) and ending measurements as late as  
148 the last hour of the day. One of the challenges is that the multiple lidar datasets are not always uniform; although most of the  
149 profile curtains began at or around 08:00 EDT, the lidar measurements commence and conclude at different times. At the time  
150 of these campaigns, the lidar data retrieval was constrained by the availability of personnel as well as the availability of

151 electricity in remote areas. ~~(at time of writing, the lidar instrument systems have been updated and are now more fully~~  
152 ~~automatized for use during succeeding campaigns removing such constraints).~~ Due to this constraint, the 91 lidar curtains  
153 range from as short as a 6-hour window to a full 24-hour window. Similarly, the profile curtains do not have an exact uniform  
154 altitude range either. In the processing of the lidar data, some measurements may be filtered out and removed due to issues,  
155 such as clouds, which can influence and degrade the retrieval leaving some blocks of empty data within the vertical altitude  
156 dimension. When the cloud conditions are perfect, the limiting factor for the altitude is the solar background: the UV from the  
157 sun is a source of noise that prevents the detection of the low level of backscattered photons. For LMOL, this means that the  
158 maximum altitude is about 10 km AGL at night (Gronoff et al., 2021) and lowered to about 4 km AGL at solar noon (worse  
159 conditions possible for the summer in the continental U.S. resulting in below 4 km AGL). This results in a general scarcity of  
160 O<sub>3</sub> measurements above 4000 m AGL for most of the vertical profile curtains. Lidars still have limitations that prove to be a  
161 complication e.g., noise signal and manual operations. At the time of writing, the operative limitation has been addressed and  
162 the lidars are now more fully automatized ~~for use during succeeding campaigns removing such constraints~~ ~~which removes some~~  
163 ~~of the difficulty.~~

164

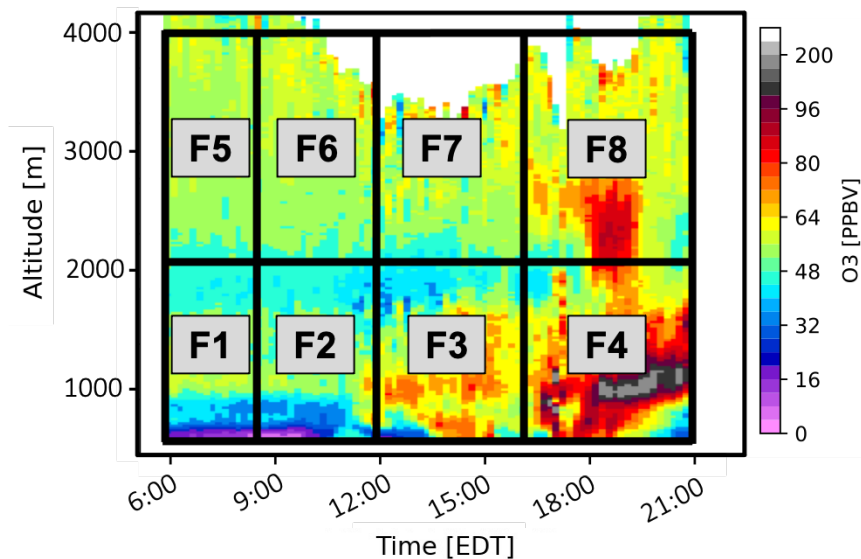
## 165 2.2.2 Clustering approach and application

166 ~~To facilitate the comparison of the 2-D O<sub>3</sub> profile curtains and the air quality model simulations~~ To characterize coastal  
167 O<sub>3</sub>, we used a cluster analysis to categorize the behavior of the tropospheric O<sub>3</sub> captured in the profile curtains. Clustering  
168 methods are commonly used in air quality and atmospheric studies to group and characterize large datasets (Darby, 2005;  
169 Alonso et al., 2006; Christiansen, 2007; Davis et al., 2010; Stauffer et al., 2018). In our previous work, we have successfully  
170 used clustering methods to automatically characterize diurnal patterns of surface winds and surface O<sub>3</sub> in the Houston-  
171 Galveston-Brazoria area that proved to perform better than a rudimentary quantile method to reveal the dependence of surface  
172 O<sub>3</sub> variability on local and synoptic circulation patterns on the Gulf Coast (Bernier et al., 2019; Li et al., 2020)

173 In evaluating the structure of the lidar measurements and working within measurement limitations (described in Sect.  
174 2.2.1) from the three air quality campaigns, we developed a method to cluster multi-dimensional O<sub>3</sub> profile curtains using K-  
175 Means clustering algorithm. Input features (seed values) were rationally established to best represent the behavior of O<sub>3</sub>  
176 temporally and vertically without including an excessive amount of input features, which can weaken the results of clustering  
177 (discussed in detail in Sect. S1, in Supplementary Material). With the goal of evaluating lower level tropospheric O<sub>3</sub> and based  
178 on description of the structure and constraints of the lidar measurements, the features were tailored to the altitude range 0 –  
179 4000 m AGL and time range of 06:00 EDT – 21:00 EDT.

180 Figure 2 illustrates the 8 features that represent the slabs of altitude and time used in the cluster analysis. For each O<sub>3</sub>  
181 profile curtain (total of 91), we calculated the average O<sub>3</sub> from the following time and altitude range: Features 1 – 4 altitudes  
182 range from 0 – 2000 m; Features 5 – 8 altitudes range from 2000 – 4000 m. The two altitude ranges were determined to best  
183 represent different O<sub>3</sub> transport events although they do not explicitly represent these layers. For Features 1 – 4, O<sub>3</sub> would most  
184 likely primarily be affected by local production and pollution transport while for Features 5 – 8, O<sub>3</sub> would more likely be

185 associated with long range transport (e.g., interstate). As planetary boundary layer growth (PBL) in coastal regions do not  
186 usually reach altitudes greater than 2000 m, mixing between the boundary layer and free troposphere would presumably take  
187 place within the low-level altitude bin. Additional attention to the PBL in the selecting of low versus mid-level features for the  
188 clustering will be investigated in future work. For clarity, we will use the terms low-level and mid-level features to address the  
189 two altitude subsets e.g., Features 1 – 4 and 5 – 8, respectively. Feature 1 and 5 time range from 06:00 – 08:00 EDT; Feature  
190 2 and 6 from 08:00 – 12:00 EDT; Feature 3 and 7 from 12:00 – 16:00 EDT; and Feature 4 and 8 from 16:00 – 21:00 EDT. The  
191 four subset time ranges were indicated to best represent features that characterize the common diurnal behavior of O<sub>3</sub>.



192  
193 **Figure 2.** Clustering method developed for clustering vertical O<sub>3</sub> profiles taken from lidar measurements. The color coding  
194 shows a typical day of lidar measurements of O<sub>3</sub> profiles on ~~August 6 August~~, 2018, from the LMOL at Westport, CT during  
195 the LISTOS Campaign. F1 – F8 indicate the time and altitude range of the eight features used for the clustering algorithm.

196  
197 The features were evaluated for cluster tendency, essentially to confirm our dataset contained meaningful clusters  
198 (discussed in detail in Sect. S2). ~~One statistical approach was used to test the dataset called Hopkins statistic which measures~~  
199 ~~whether there is uniform distribution (spatial randomness) within the dataset (Lawson and Jurs, 1990). The results calculated~~  
200 ~~using the Hopkins statistic concluded a value higher than 0.75 (actual = 0.77) which by this standard indicates a clustering~~  
201 ~~tendency at the 90 % confidence level.~~ Evaluating different feature options did not lead to better statistical results than with  
202 the final chosen features. ~~To visualize the cluster tendency of our dataset, we applied the algorithm of the visual assessment of~~  
203 ~~cluster tendency (VAT) approach (Bezdek and Hathaway, 2002) which uses the Euclidean distance measure to compute the~~  
204 ~~dissimilarity matrix in the dataset and creates an ordered dissimilarity matrix image. Figure S1 shows the VAT approach results~~  
205 ~~which indicates high similarity (red) and low similarity (blue) and confirms a cluster structure (not random) within our dataset.~~



206 Since the choice of clustering algorithm is subjective, we chose K-means clustering for its simplicity and widespread use.  
207 To use the K-Means clustering algorithm, the optimal number of clusters based on your dataset must be chosen beforehand  
208 (Sect. S2). ~~For this study, the package Nbelust (Charrad et al., 2014) in R was used, which applies 30 indices for determining~~  
209 ~~the optimal number of clusters. Using this package, as well as testing the quality of the clustering results using the silhouette~~  
210 ~~method (Kaufman & Rousseeuw, 1990).~~ We selected six clusters as the optimal number of clusters. Since the K-Means  
211 clustering algorithm is based on the Euclidean distance to each centroid, the input data was normalized (to a mean of zero and  
212 standard deviation of one) to ensure each feature is given the same importance in the clustering (Aksoy & Haralick, 2001;  
213 Larose, 2005).

214 ~~The clustering analysis initially identified six clusters. The resulting six clusters (described fully in Sect. 3.2) represent~~  
215 ~~clusters of regularly observed lidar O<sub>3</sub> curtains for the regions of our study during the campaign periods. Only one date was~~  
216 assigned to Cluster 6 (16 June 2018): the lidar profile curtain on this day (Figure S16) shows a large fraction of data missing,  
217 and the available data have relatively high O<sub>3</sub> throughout the lowest 3 km, which is different from other clusters. Therefore,  
218 we consider Cluster 6 to be an outlier and will not be included in the subsequent analysis.

219

220

### 221 2.2.3 Missing data

222 Although the input features were tailored based on the structure of the lidar measurements, the remaining data still had  
223 missing data points. In performing a quick evaluation on the 8 input features (Figure S65), we found that Features 1, 4, 5, and  
224 8 had the most missing data while Features 2, 3, 6, and 7 had few or zero cases of missing data. This means that the earlier  
225 morning measurements (06:00 – 12:00 EDT) and the later evening measurements (16:00 – 21:00 EDT) had the most cases of  
226 missing data points. This is plausible as the campaign teams were best able to retrieve clear measurement during  
227 midday/evening hours (12:00 – 16:00 EDT). As a result, 51 out of 91 O<sub>3</sub> profile curtains had at least one missing data point  
228 (feature) throughout the individual profile curtain.

229 A common practice for dealing with missing data is complete case analysis (CCA), in which observations with missing  
230 values are completely ignored, leaving only the complete data to cluster. CCA can be inefficient as it introduces selection bias  
231 since the sample data no longer retains the state of the original full dataset (Donders et al., 2006; Little & Rubin, 2014). When  
232 we applied CCA, there were only 40 O<sub>3</sub> profile curtains of complete data, removing over half of the study profiles. Instead,  
233 we used a more comprehensive solution – imputation – that yields results (Donders et al., 2006). For this study we used the  
234 single imputation (SI) technique, *knnImputation*, which uses the k-nearest neighbors and searches for the most similar cases  
235 and uses the weighted average of the values of those neighbors to fill the missing data (Torgo, 2010). Essentially, this method  
236 selects the days that have the most similar profile curtain to any profile which has missing data points and uses those real data  
237 points to calculate a weighted mean that will fill in the missing data. We acknowledge using an imputation method on the  
238 dataset will possibly introduce a bias which is difficult to quantify, but this allows us to utilize the use of the full all 91 O<sub>3</sub>  
239 profile curtains ~~of O<sub>3</sub> data~~. The silhouette method was used to test the quality of the newly imputed dataset and proved to be



240 no worse, nor better, than the CCA (*real data*) results. Therefore, the dataset was first imputed using SI to create a complete  
241 dataset and then the clustering method described in the sect. before (2.2.2) was applied to the complete imputed dataset.

242

### 243 **2.3. Model simulations**

244 The offline GEOS-Chem chemical-transport model (CTM) was utilized to simulate the spatial and temporal variability  
245 of coastal O<sub>3</sub> in the Chesapeake Bay and Long Island Sound during the time of the campaigns. The GEOS-Chem model is a  
246 global 3-D CTM driven by assimilated meteorological data from the NASA Global Modeling and Assimilation Office  
247 (GMAO). Our simulations were driven by reanalysis data from Modern-Era Retrospective analysis for Research and  
248 Applications, Version 2 (MERRA-2; Gelaro et al., 2017). We ran a nested GEOS-Chem (v12-09) simulation at 0.5° x 0.625°  
249 horizontal resolution over the eastern portion of North America and adjacent ocean (90 – 60°W, 20 – 50°N), using lateral  
250 boundary conditions updated every three hours from a global simulation with 2° x 2.5° horizontal resolution. The nested  
251 GEOS-Chem simulation was run with 72 vertical levels from 1013 to 0.01 hPa. Since the study focuses on the altitude range  
252 0 – 4000 m, the first 20 vertical levels from GEOS-Chem were used with 14 levels within the boundary layer ( $\leq 2000$  m). The  
253 nested simulation was conducted for the study periods June – September 2017 and April – August 2018. We used the standard  
254 “out-of-the-box” unmodified default settings from the tropospheric chemistry chemical mechanism (tropchem) with global  
255 anthropogenic emissions from the Community Emissions Data System (CEDS) inventory (McDuffie et al, 2020) and U.S.  
256 Environmental Protection Agency (EPA) National Emissions Inventory (NEI) 2011 for monthly mean North American  
257 regional emissions (EPA NEI, 2015).

258 We also used results from NASA’s near real-time forecasting system, GEOS-CF, an online GEOS-Chem simulation (v12-  
259 0-1) from GMAO ([https://gmao.gsfc.nasa.gov/-weather\\_prediction/GEOS-CF/](https://gmao.gsfc.nasa.gov/-weather_prediction/GEOS-CF/)) with GEOS coupled to the GEOS-Chem  
260 tropospheric-stratospheric unified chemistry extension (UCX) and run at a high spatial resolution of 0.25°, roughly 25 km  
261 (Keller et al., 2021, Knowland et al., 2021). The vertical resolution for GEOS-CF is interpolated onto 72 vertical levels from  
262 1000 to 10 hPa. Since the study focuses on the altitude range 0 – 4000 m, the first 21 vertical levels from GEOS-CF were used  
263 with 14 levels within the boundary layer ( $\leq 2000$  m). Prior to the launch of the 12z five-day forecast, GEOS-CF produces daily  
264 global, 3-D atmospheric composition distributions using the GEOS meteorological replay technique (Orbe et al., 2017), and  
265 this study makes use of these historical estimates, made available to the public for the period since January 2018. Therefore,  
266 the GEOS-CF results shown in this study only include the dates from OWLETS-2 and LISTOS campaigns, since they both  
267 occurred in 2018.

268 While both model simulations use similar versions of GEOS-Chem chemistry, there are noteworthy differences to keep  
269 in mind during the analysis of the clustering. The main differences between the two models are (1) GEOS-Chem is an offline  
270 CTM using archived meteorology, while GEOS-CF simulates atmospheric composition simultaneously with meteorology  
271 (online); (2) the spatial resolution of the GEOS-CF model (0.25°) is higher than GEOS-Chem (0.5° x 0.625°); and (3) the  
272 GEOS-CF model runs with Harmonized Gridded Air Pollution (HTAP; v2.2; base year 2010) anthropogenic emissions from

273 the Emission Database for Global Atmospheric Research (EDGAR), while GEOS-Chem was run with CEDS anthropogenic  
274 emissions (base year 2014). These imperative differences can lead to disparities in the following results.

275

### 276 3. Results & Discussion

#### 277 3.1 Overview of the 2-D O<sub>3</sub> curtain clusters

278 ~~The clustering results reveal distinctive characterized O<sub>3</sub> behavior during the three campaigns in which O<sub>3</sub> concentrations~~  
279 ~~vary across the clusters. As previously mentioned in Sect. 2.2.3, the clustering analysis initially identified six cluster groups~~  
280 ~~from the O<sub>3</sub> profile curtains. Only one date was assigned to Cluster 6 (16 June 2018): the lidar profile curtain on this day~~  
281 ~~(Figure S6) shows a large fraction of data missing, and the available data have relatively high O<sub>3</sub> throughout the lowest 3 km,~~  
282 ~~which is different from other clusters. Therefore, we consider Cluster 6 to be an outlier and will not include it in the subsequent~~  
283 ~~analysis.~~

284 The clustering results reveal distinctive characterized O<sub>3</sub> behavior during the three campaigns in which O<sub>3</sub> concentrations  
285 vary across the clusters. Various O<sub>3</sub> and surface meteorological parameter cluster statistics for the ~~remaining~~ five clusters are  
286 summarized in Table 1. With only 5 of the 2-D profile curtains assigned, Cluster 5 depicts the least common O<sub>3</sub> behavior  
287 during the campaigns. On the other hand, Cluster 3 is the most common O<sub>3</sub> behavior during the campaigns with 28 profile  
288 curtains assigned to this cluster. Following Cluster 3, Cluster 1 is the next most common cluster with 25 profile curtains.  
289 Cluster 2 and Cluster 4 fall in the middle with 14 and 18 profile curtains assigned to the cluster numbers, respectively.

290

291

292 Cluster #	a) No. of vertical profiles	293 b) O <sub>3</sub> Max (ppb)	294 c) O <sub>3</sub> Min (ppb)	295 d) T avg. (min; max) (°F)	296 e) WS avg. (min; max) (m s <sup>-1</sup> )
297 1	25	86.5	42.2	74.1 (67.8; 86.4)	1.5 (0.5; 2.8)
298 2	14	72.8	28.9	71.6 (64.0; 83.9)	1.6 (0.6; 2.9)
299 3	28	86.6	34.2	77.2 (67.0; 87.6)	1.3 (0.5; 2.4)
300 4	18	97.8	44.1	78.4 (68.0; 90.4)	1.2 (0.4; 2.3)
301 5	5	67.7	29.1	74.5 (66.8; 74.5)	1.2 (0.3; 3.4)

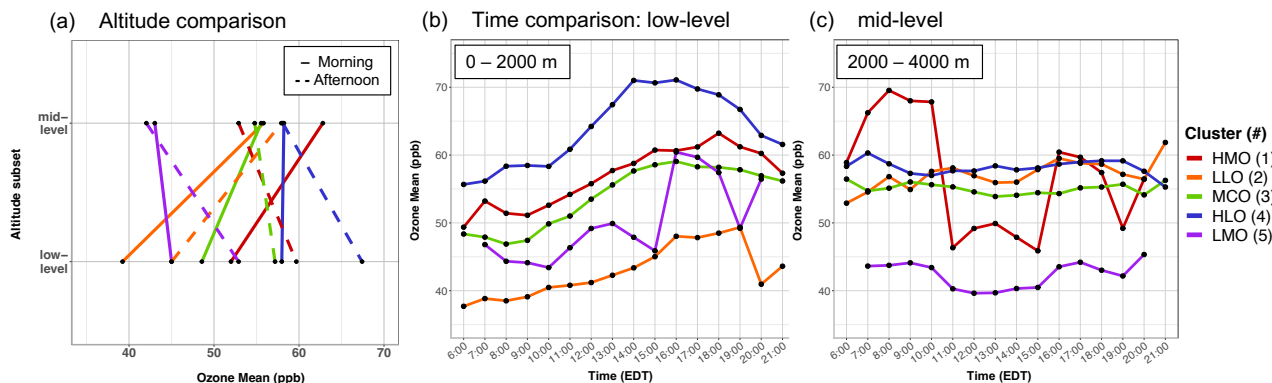
300

301 **Table 1.** Lidar vertical O<sub>3</sub> profile cluster statistics: a) total number of vertical profiles; b) O<sub>3</sub> maximum; c) O<sub>3</sub> minimum O<sub>3</sub>;  
302 AQS monitoring station cluster mean d) surface temperature and e) wind speed; minimum and maximums in parenthesis. The  
303 statistics and averages were derived from the total number of profile curtains assigned to each cluster.

304

305 The five clusters were distinguished by the varying O<sub>3</sub> concentrations between the low-level and mid-level as well as  
306 diurnal variations (Figure 3). ~~In Figure 3a-quantifies the between-cluster differences w\_~~ We separate the data by the two altitude

307 subsets (low and mid-level) and by ~~two time subsets~~ (morning (0=6:00 – 12:00) and afternoon (=12:00 – 21:00) to quantify  
 308 ~~the between-cluster differences for lucidity as the majority of the cluster differences are contrasted between these subsets.~~ In  
 309 the low-level, all five clusters exhibit the common O<sub>3</sub> diurnal pattern where surface O<sub>3</sub> is titrated overnight and reaches a  
 310 minimum but then is quickly exacerbated with the increase of sunlight throughout the day and typically peaks after midday  
 311 (Figure 3b). The extent of this common diurnal pattern varies by cluster.  
 312



313  
 314 **Figure 3.** Lidar O<sub>3</sub> cluster average comparisons (five clusters depicted in colors). a) Altitude comparison of mean O<sub>3</sub> averaged  
 315 over time: morning hours from 6:00 – 12:00 (solid line) and afternoon hours from 12:00 – 21:00 (dashed lines). Time  
 316 comparison of mean hourly O<sub>3</sub> split between the b) low-level and c) mid-level.

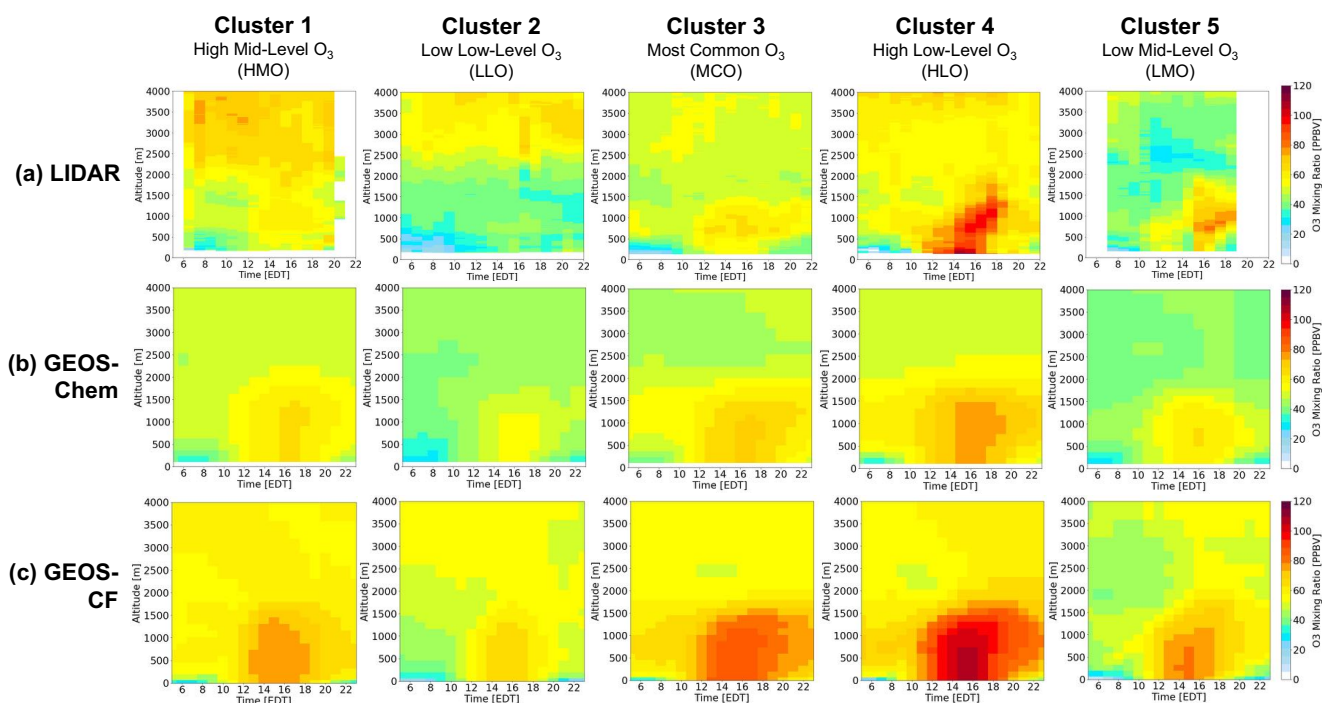
317  
 318 Cluster 1 in the low-level has the second highest morning and afternoon O<sub>3</sub> average (52 and 59 ppb) and in the mid-level  
 319 the highest morning O<sub>3</sub> average (64 ppb) (Figure 3a). Cluster 1 also exhibits the most unique pattern of mid-level O<sub>3</sub> (Figure  
 320 3c), with the highest concentrations found in the early morning and an uncharacteristic plunge to lower O<sub>3</sub> concentrations from  
 321 11:00 – 15:00 EDT. This is contrary to the other clusters which do not show much O<sub>3</sub> variation temporally in the mid-level.  
 322 The majority of the individual profile curtains assigned to Cluster 1 show concentrated early morning residual layers in the  
 323 mid-level that diffuse after the morning, which is distinctive to the other clusters. In the low-level, Cluster 2 has the lowest  
 324 morning and afternoon O<sub>3</sub> average among the clusters (39 and 45 ppb) with moderate mid-level O<sub>3</sub> concentrations. Cluster 3  
 325 has the most uniform vertical O<sub>3</sub> extent between the low and mid-level (Figure 3a), in contrast to the other clusters that differ  
 326 greatly in O<sub>3</sub> concentrations between the two altitude subsets. Cluster 4 has the highest morning and afternoon O<sub>3</sub> averages (59  
 327 and 68 ppb) in the low-level, reaching > 70 ppb temporally (Figure 3b). Finally, Cluster 5 has, considerably, the lowest morning  
 328 and afternoon O<sub>3</sub> averages (42 and 43 ppb) in the mid-level, almost 10 ppb lower than the other clusters. Cluster 5 does not  
 329 have a smooth-evolving O<sub>3</sub> diurnal pattern in the lower level (Figure 3b), which can be attributed to the averaging of only five  
 330 different profile curtains that were assigned to this cluster (Table 1).

331 Figure 4a illustrates the mean lidar O<sub>3</sub> 2-D profile curtains for each of the clusters. For Cluster 1, 3, 4, and 5, higher O<sub>3</sub>  
 332 concentrations in the low-level are captured during afternoon/evening time (12:00 – 21:00 EDT), with the highest low-level

333 O<sub>3</sub> in Cluster 4 (> 70 ppb). This behavior follows the common diurnal pattern of O<sub>3</sub>, that was distinguishable in Figure 3b. This  
 334 common O<sub>3</sub> growth reaches vertically to approximately 1500 m for each of the clusters but is generally contained below 2000  
 335 m. Differing from the low-level O<sub>3</sub> behavior, mid-level O<sub>3</sub> is generally less variable in magnitude throughout the entire profile  
 336 curtain (except for Cluster 1; see Figure 3a). The highest O<sub>3</sub> concentrations for the mid-level are exhibited in Cluster 1, 2, 3,  
 337 and 4, with the highest mid-level O<sub>3</sub> in Cluster 1 during the early morning hours ( $\geq 70$  ppb).

338 Following the descriptions above, each cluster is given a nomenclature according to their unique characteristics. Cluster  
 339 1 is termed as the highest mid-level O<sub>3</sub> (HMO) cluster; Cluster 2 as the lowest low-level O<sub>3</sub> (LLO) cluster; Cluster 3 is the  
 340 most common O<sub>3</sub> (MCO) cluster; Cluster 4 is the highest low-level O<sub>3</sub> (HLO); Cluster 5 is the least common and lowest mid-  
 341 level O<sub>3</sub> (LMO) cluster. The O<sub>3</sub> variability represented and justified above is what led to the successful clustering of the lidar  
 342 O<sub>3</sub> 2-D profile curtains.

343



344

345 **Figure 4.** Cluster-mean O<sub>3</sub> vertical profile results by cluster assignment (1- 5) and arranged: a) LIDAR; b) GEOS-Chem  
 346 simulation; and c) GEOS-CF simulation.

347

348 ~~The clustering analysis results provided a characterization of O<sub>3</sub> behavior that transpired during these three campaigns.~~  
 349 Figure 3b and 3c indicate each cluster represents a different O<sub>3</sub> evolution pattern, likely related to different photochemical or  
 350 transport regimes. This kind of evaluation is useful in that it combines O<sub>3</sub> information from both temporal and vertical  
 351 dimensions. For example, the HLO cluster reveals a unique low-level case in which high O<sub>3</sub> concentrations at a high elevation

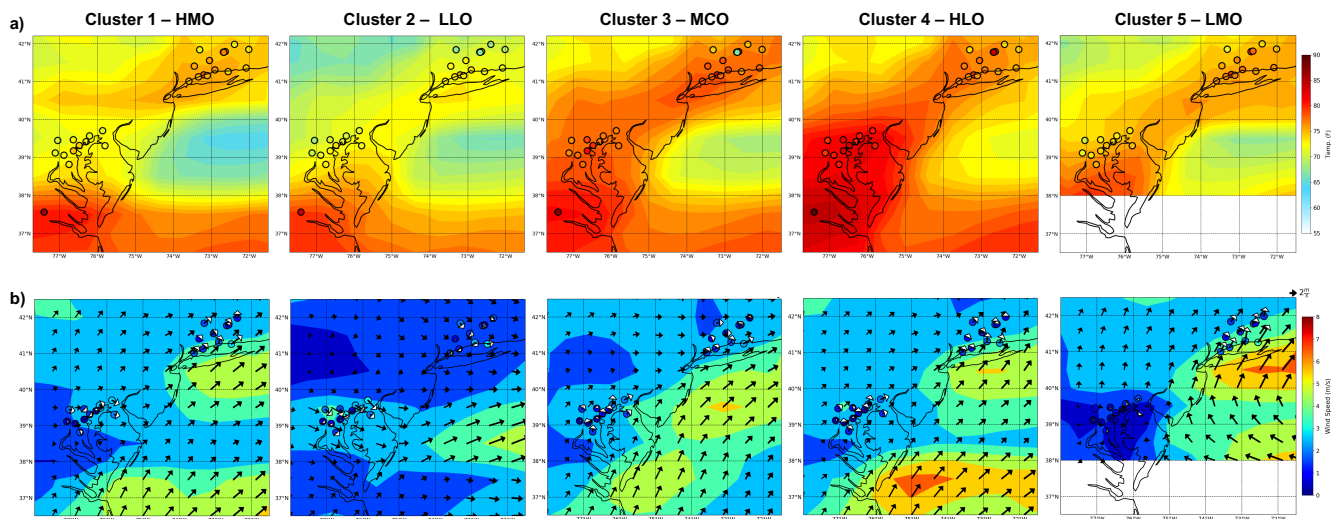
352 (~1000 m) are captured early in the temporal profile that translate to the higher O<sub>3</sub> concentrations at the surface later in the  
 353 evening. For example, the HLO cluster reveals the specific case in which higher O<sub>3</sub> is captured early in the temporal profile in  
 354 the low-level and translates to the higher O<sub>3</sub> captured in the low-level as well. The mean profile curtains show higher  
 355 background O<sub>3</sub>, indicating these cases did not have “clean air” to begin with which can allow a greater accumulation in the  
 356 low-level in the afternoon. This is an example of how this type of clustering analysis, if applied, could demonstrate background  
 357 O<sub>3</sub> in the similar case studies. In another example, several profile curtains assigned to the HMO cluster indicate concentrated  
 358 residual layers in the mid-level and possible entrainment to the surface as the day progressed. To prove this feature, vertical  
 359 velocity and vertical velocity variance data would be needed but the knowledge that a clustering approach is able to pinpoint  
 360 highlight these features that could only be discernible through lidar measurements proves to be useful. The clustering results  
 361 were valuable in recognizing a significant large pollution related cluster (HLO), a total of 18 out of the 91 curtain profiles  
 362 which correspond with the highest daily surface maxima measured at these sites (= 97.8 ppb) (Table 1). This cluster, on  
 363 average, exhibited a daily surface maxima up to 10 ppb greater than any of the other clusters. Discerning these higher O<sub>3</sub> cases  
 364 is imperative for mitigating severe air pollution.

365

### 366 3.2. Cluster surface analysis

367 To support the lidar clustering results, daily averaged meteorological surface observations from AQS stations nearest to  
 368 the lidar locations pertaining to the campaign period and GEOS-Chem surface model output were evaluated in regard to the  
 369 five clusters. Figure 5 shows the cluster mean surface temperature from AQS stations and GEOS-Chem model as well as the  
 370 simulated wind speed and direction. The average surface temperature from each station is represented as the circular markers  
 371 while the simulated temperatures are represented as the spatial contour and the simulated wind speed (m s<sup>-1</sup>) and direction as  
 372 arrows. Cluster average, minimum, and maximum AQS surface temperature and wind speed can be found in Table 1d, e.

373



374

375 **Figure 5.** Cluster averaged meteorological surface AQS station observations and GEOS-Chem model results. a) Surface  
376 temperature observations represented as the circular markers and simulated surface temperatures represented as the spatial  
377 contour (top-panel). b) Surface wind speed and direction observations represented as the circular markers and white arrows  
378 and simulated wind speed and direction represented as spatial contour and black arrows (bottom-panel).

379

380 In general, the surface meteorological conditions agree with our knowledge of transport and O<sub>3</sub> production that would  
381 lead to each of the five clustered lidar O<sub>3</sub> profile curtains. It is evident that the clusters with the highest surface O<sub>3</sub> (HMO,  
382 MCO, and HLO) all share a predominant offshore, westerly wind. Furthermore, MCO and HLO presented higher overall  
383 observed and simulated surface temperatures compared to the other clusters (Figure 5a). ~~Observed and simulated wind speeds~~  
384 ~~reveal slightly lower average wind speeds and primarily continental wind flow for both clusters as well (Figure 5b).~~ These  
385 meteorological conditions are conducive to a higher production of surface O<sub>3</sub> concentrations which validates the higher O<sub>3</sub>  
386 found in the low-level results (Figure 3b, 4a).

387 Conversely, the lowest surface temperatures are found in LLO. Lower surface temperatures are also indicative of low  
388 vertical mixing due to less generation of convection which can reduce any possible descending O<sub>3</sub> from aloft. Relatively calm  
389 wind speeds, ~~and~~ lower temperatures, ~~and indicate~~ other possible meteorological factors such as high cloud cover ~~that~~ could  
390 have contributed to the lower O<sub>3</sub> concentrations in LLO. Although surface O<sub>3</sub> concentrations in LMO reach higher levels later  
391 in the day, first at 13:00 EDT and then again at 16:00 EDT, the rest of the temporal profile stays below moderate levels.  
392 Average temperatures for LMO are moderately high but, in contrast, the average wind speed is higher (specifically over the  
393 Long Island Sound) and unique to the other clusters, wind direction is predominantly onshore (Easterly – Southerly). This  
394 prevalent onshore flow indicates a transport of cleaner marine air which corroborates the lower surface O<sub>3</sub> levels. LMO did  
395 not have any profile curtains assigned from OWLETS-1 which is why data for the lower Chesapeake Bay area is not shown in  
396 Figure 5.

397 There was only one occurrence during the dates in which the lidar instruments were operating in which there was a  
398 recorded maximum daily 8-hour average (MDA8) O<sub>3</sub> exceedance (> 70 ppbv). This exceedance date is 25 May 2018 in which  
399 3 AQS sites in the LISTOS region measured MDA8 O<sub>3</sub> of 73, 72, and 72 ppbv. This curtain profile was assigned to the HMO  
400 cluster (Cluster 1), the cluster with high O<sub>3</sub> in the mid-level and moderate O<sub>3</sub> in the low-level and near the surface. Since the  
401 AQS stations applied here were the nearest stations to the lidar instrument placements, the MDA8 O<sub>3</sub> captured by the AQS  
402 stations do not necessarily reflect the high O<sub>3</sub> concentrations capture by the lidars near the surface.

403

### 404 3.3. Evaluating the GEOS-Chem and GEOS-CF model

405 In this sect. the model results from GEOS-Chem and GEOS-CF will be compared to the lidar data using the five lidar O<sub>3</sub>  
406 profile clusters discussed in Sect. 3.1. Both model results were sampled in an equal manner, in which we extracted the same  
407 cluster date assignments from the lidar clusters and created mean vertical profiles based on the model results. This allowed us  
408 to evaluate the model performance based on the five characterized O<sub>3</sub> lidar clusters. As mentioned previously, the GEOS-CF



409 simulation data is not available for 2017. Thus, the results shown subsequently will only include GEOS-CF results from 2018  
410 (only dates from the OWLETS-2 and LISTOS campaigns). The GEOS-Chem simulation results include both years thus all  
411 three campaign duration periods.

412

### 413 3.3.1 Overall model performance

414 Figure 4b and 4c depict the simulated cluster-mean O<sub>3</sub> profile curtains from GEOS-Chem and GEOS-CF, mirroring the  
415 mean lidar profile curtains in Figure 4a. For all clusters in the low-level, both models simulate a consistent accumulation of  
416 O<sub>3</sub> near the surface after 12:00 EDT, mirroring the O<sub>3</sub> common diurnal pattern depicted in mean lidar profile curtains in Figure  
417 4a. However, the extent the models simulate is often higher in magnitude than the observations, specifically GEOS-CF  
418 consistently predicting the accumulation at a higher magnitude than GEOS-Chem. In the mid-level, both models simulate  
419 much less O<sub>3</sub> variability than what is captured in the lidar observations. Figure 4b and 4c clearly show how the models struggle  
420 to reproduce any mid-level O<sub>3</sub> pattern or variability that is relayed in the lidar observations. ~~This is in contrast to the low-level~~  
421 ~~where the models are able to reproduce the common diurnal pattern of O<sub>3</sub>. With the lidar data providing a full temporal and~~  
422 ~~vertical profile curtain of O<sub>3</sub> behavior and development, we are able to indicate areas where the models struggle such as in this~~  
423 ~~case in the mid-level.~~

424 We first evaluate overall correlation and biases between the model and lidar data, disregarding the specific clusters. The  
425 overall correlation between the models and the lidar data ~~is evaluated by~~ ~~disregarding the specific clusters, based on~~ the two  
426 altitude subsets as the performances differ considerably between low-level and mid-level for both GEOS-Chem (Figure S7a)  
427 and GEOS-CF (Figure S7b) ~~(mean normalized biases found in Table S1).~~ ~~The mean normalized biases for the five clusters~~  
428 ~~displayed in Table S1 (in Supplementary Material) were calculated from the total vertical and diurnal averages separated by~~  
429 ~~low-level and mid-level.~~ For both models, overall low-level O<sub>3</sub> correlation rounds to 0.70, signifying a strong relationship  
430 between the model simulations and the lidar observations (Figure S7 - top panel). This indicates that both models can simulate  
431 the development and pattern of O<sub>3</sub> well in the low-level. Overall, GEOS-Chem performs well in simulating low-level O<sub>3</sub> with  
432 a lower non-systematic normalized bias ranging from -0.10 to +0.13 ~~for the five clusters~~. Thus, based on the lower bias, GEOS-  
433 Chem also fairs well simulating the magnitude of low-level O<sub>3</sub>. ~~For all clusters~~ Overall, GEOS-CF overestimates the average  
434 magnitude of low-level O<sub>3</sub> with a systematic high positive normalized bias ranging from +0.30 to +0.67. This consistently high  
435 bias reveals that GEOS-CF generally ~~is unable to simulate~~ struggles to simulate low-level O<sub>3</sub> magnitude.

436 For the mid-level, the overall correlation reveals that GEOS-CF and GEOS-Chem both have a weak relationship with the  
437 lidar (R = 0.22 and R = 0.12, respectively) (Figure S7 - bottom panel). This indicates that neither model ~~is able to can~~ simulate  
438 mid-level O<sub>3</sub> pattern well. GEOS-Chem consistently underestimates the magnitude of mid-level O<sub>3</sub> with a systematic high  
439 negative normalized bias ranging from -0.44 to -0.18, ~~for all clusters~~, while GEOS-CF has a lower and non-systematic  
440 normalized bias ranging from -0.22 to 0.28. Overall, both models are not able to simulate the O<sub>3</sub> variability nor magnitude  
441 well in the mid-level. The overall analysis ~~in this sect.~~ provides a fundamental but condensed assessment of model

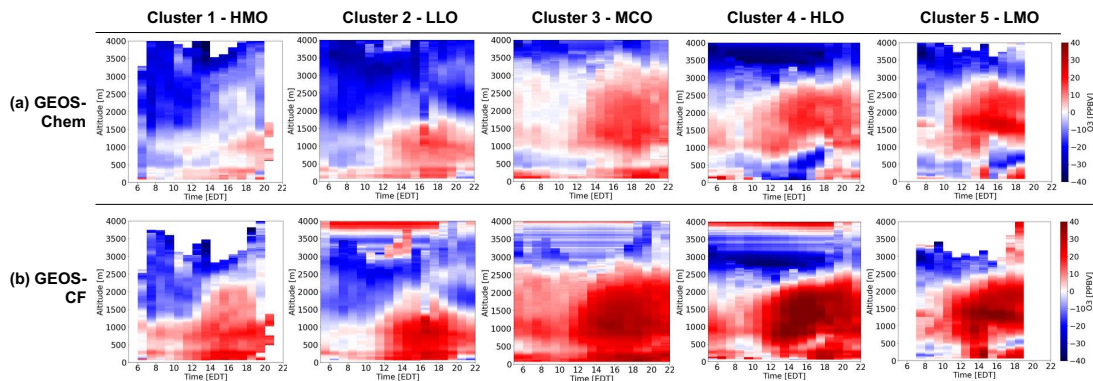


442 performance. ~~In the next sect., the cluster specific differences reveal additional model performance insight that would be~~  
443 ~~conceivably overlooked when evaluating overall performance.~~

### 445 3.3.2 Model evaluation based on lidar clusters

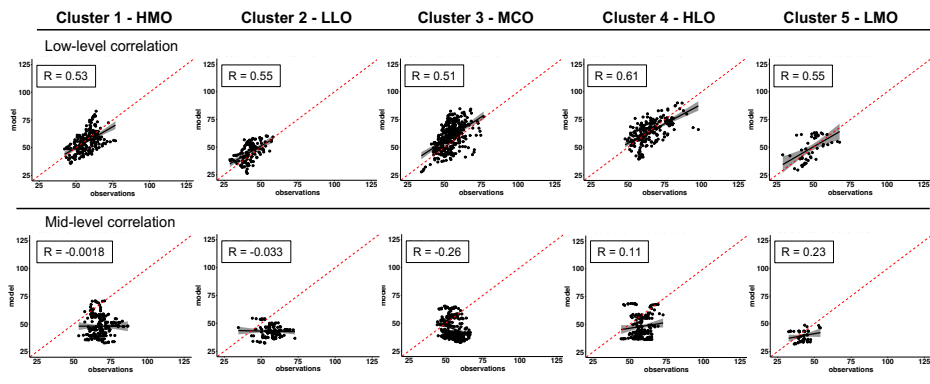
446 ~~As demonstrated in Sect. 3.3.1, we can evaluate summarized model performance and come to the simple conclusion that~~  
447 ~~both models fairly simulate low level O<sub>3</sub> but struggle to simulate mid level O<sub>3</sub>. However, a systematic and comprehensive~~  
448 ~~understanding of the different photochemical regimes in these coastal regions and how models simulate varying behaviors~~  
449 ~~requires more insight. In this section we discuss s~~Significant cluster by cluster differences in model performance that are  
450 unmasked by the clustering approach. ~~in evaluating the models based on the established O<sub>3</sub> behavior cases. To better explain~~  
451 ~~the side-by-side comparison quantify the results illustrated~~ in Figure 4, ~~we show~~ spatial O<sub>3</sub> differences (model – lidar  
452 observations) for each cluster ~~were derived~~ (Figure 6) as well as individual cluster correlation (Figure 7, Table S1) ~~(subsequent~~  
453 ~~cluster calculated normalized biases and correlation can be found in Table S1). Subsequent mean normalized biases (Table~~  
454 ~~S1) were calculated from the total vertical and diurnal averages separated by low-level and mid-level. Evaluating the individual~~  
455 ~~cluster biases and correlation reveal more in depth model discrepancies as well as areas where the models perform well.~~

Spatial O<sub>3</sub> Difference: model – lidar observations

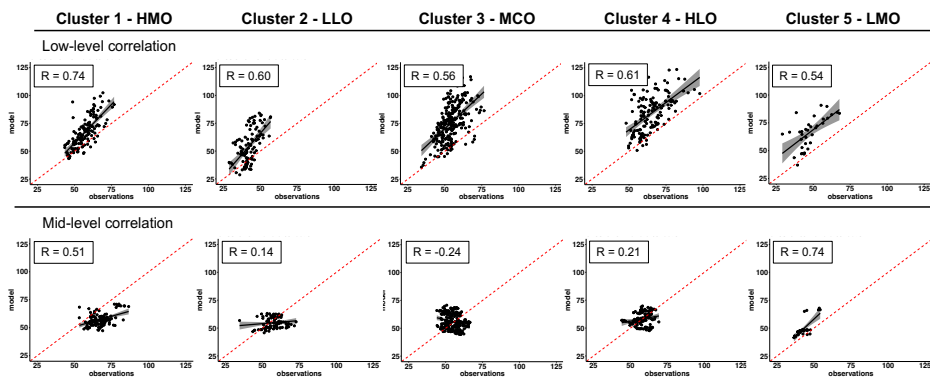


457  
458 **Figure 6.** Mean profile curtain spatial O<sub>3</sub> difference (model – lidar observations) for each cluster (1 – 5). GEOS-Chem  
459 differences (a) and GEOS-CF differences (b).

(a) GEOS – Chem model



(b) GEOS – CF model



460

461 **Figure 7.** O<sub>3</sub> correlation between lidar observations and a) GEOS-Chem model simulation results and b) GEOS-CF model  
462 results by each cluster split by low-level (top panel) and mid-level (bottom panel).

463

464 In the low-level, GEOS-CF has a similar performance ability for the HMO, HLO, and LMO clusters with high positive  
465 biases at +0.30, +0.41, and +0.45 respectively. These higher biases imply GEOS-CF has difficulty capturing moderate O<sub>3</sub>  
466 ~~cases concentrations below 2000 m~~ (HMO and LMO) as well as ~~the in the~~ high O<sub>3</sub> cases (HLO) ~~below 2000 m~~. GEOS-CF  
467 also has a high positive bias (+0.50) in the LLO cluster indicating ~~that GEOS-CF the model~~ struggles to capture the lower O<sub>3</sub>  
468 ~~concentrations cases in the low level as well~~. This is warranted as models are intended to approximate and are not usually able  
469 to capture extremes (high or low) ~~but GEOS-CF also seems to struggle capturing moderate cases as well~~. In the low-level,  
470 GEOS-Chem has the best performance (minimal ~~-~~0.04 bias and strong correlation, R = 0.61) in HLO, ~~which is~~ the cluster  
471 with the highest low-level O<sub>3</sub> accumulation (~~refer to Figure 4a~~). ~~The and the~~ second-best performance (~~minimal +0.07 bias and~~  
472 ~~fair correlation, R = 0.55~~) for GEOS-Chem in the low-level follows closely behind in LLO (~~minimal +0.07 bias and fair~~  
473 ~~correlation, R = 0.55~~) in LLO, the cluster with the lowest O<sub>3</sub> accumulation. These results ~~suggest GEOS-Chem performs well~~  
474 ~~in cases of high O<sub>3</sub> as well as cases of low O<sub>3</sub> with a slight tendency to overpredict lower O<sub>3</sub> concentrations and underpredict~~  
475 ~~higher O<sub>3</sub> concentrations. This challenge~~es the overall assumption that models struggle to capture extreme cases ~~since GEOS-~~

476 ~~Chem actually performs best in simulating both extreme cases of high O<sub>3</sub> in HLO and, again, low O<sub>3</sub> in LLO.~~ GEOS-Chem  
477 has a similar performance for the LMO and HMO clusters with low negative biases of - 0.10 and - 0.09, respectively, =  
478 indicating GEOS-Chem the model is also able to capture ~~the moderate O<sub>3</sub> in both of these clusters well with slight~~  
479 ~~underestimations cases.~~

480 Both models perform the worst (in comparison ~~with the~~ other clusters) in the low-level in the MCO cluster with a +  
481 0.13 bias for GEOS-Chem and + 0.67 bias for GEOS-CF. As described in Sect. 3.1, MCO is the most common cluster with  
482 moderate - high average O<sub>3</sub> concentrations in the low-level (refer to Figure 3b). Although GEOS-Chem has ~~the-its~~ worst  
483 performance in the MCO cluster, it is not necessarily a poor performance. ~~The performance follows the conclusion previously~~  
484 ~~made that GEOS-Chem can fairly simulate moderate O<sub>3</sub> in the low-level although, in this case, with slight overestimations.~~  
485 Contrarily, the GEOS-CF performance in the MCO cluster reveals a more substantially high positive bias. This stands out as  
486 models are usually able to capture moderate levels (e.g., non-extreme cases). Evaluating the full temporal and vertical profile  
487 indicates that the higher GEOS-CF bias in the MCO cluster is additionally influenced by the greater overestimation of morning  
488 O<sub>3</sub>, not solely the afternoon O<sub>3</sub>. This is different to the performance in the LLO and LMO clusters where GEOS-CF also had  
489 a high positive bias in the low-level but ~~does~~ better simulate ~~testing the~~ early morning O<sub>3</sub> ~~magnitude~~. A similar conclusion can  
490 be drawn when evaluating the low-level GEOS-Chem performance. HMO, LLO, MCO, and LMO all share 'higher' biases  
491 (rounding to +/- 0.10), but the highest bias is found in the MCO cluster. This can similarly be attributed to GEOS-Chem  
492 overestimating morning O<sub>3</sub> ~~the worst~~ in the MCO cluster in contrast to the better early morning estimation in the other clusters.

493 In the mid-level, GEOS-Chem underestimates O<sub>3</sub> magnitude to the greatest extent in the HMO and the LLO cluster (both  
494 bias = - 0.44), which are both clusters with higher mid-level O<sub>3</sub> concentrations (refer to Figure 3c). GEOS-Chem performs  
495 similarly in the HLO and MCO clusters, with a negative mean bias of - 0.30 and - 0.27, respectively. This indicates that  
496 GEOS-Chem most struggles to simulate higher concentrations of O<sub>3</sub> in the mid-level. The GEOS-Chem model actually never  
497 reaches O<sub>3</sub> cluster averages greater than 50 ppb, directly divulging the greater systemic negative bias in the mid-level. GEOS-  
498 Chem simulates LMO mid-level O<sub>3</sub> magnitude the best (- 0.18 bias), which is the cluster with the lowest O<sub>3</sub> average (< 45  
499 ppb). Although for the LMO cluster GEOS-Chem has a lower bias, the correlation is still poor (R = 0.23) which indicates that  
500 the model is relatively capable of simulating mid-level O<sub>3</sub> only when the case devises lower concentrations but still fails to  
501 replicate any O<sub>3</sub> variability and pattern.

502 On the other hand, GEOS-CF does best simulating LLO, MCO, and HLO, which are all clusters with moderate O<sub>3</sub> in the  
503 mid-level ( $\geq 50$  and  $\leq 70$  ppb). GEOS-CF has the highest bias in the LMO cluster (+ 0.28), the cluster with the lowest mid-  
504 level O<sub>3</sub> magnitude ~~but =GEOS-CF~~ also has the strongest correlation in the same ~~LMO~~ cluster (R = 0.74). This is a unique  
505 case where although ~~GEOS-CF the model~~ is not able to capture ~~mid-level O<sub>3</sub> the magnitude in the mid-level~~, it is able to capture  
506 the ~~pattern variability of low O<sub>3</sub>~~ well. Comparing the full ~~multi-dimensional lidar and model mean~~ profile curtains it is evident  
507 that in the LMO cluster, the GEOS-CF model simulates ~~a similar~~ mid-level O<sub>3</sub> pattern in the morning/early afternoon fairly  
508 well that is captured in the mean lidar curtain profile. ~~The second worst performance for GEOS-CF also is the underestimation~~  
509 ~~of struggles to simulate~~ mid-level O<sub>3</sub> in the HMO cluster, contrarily the cluster with the highest mid-level O<sub>3</sub> ( $\geq 70$  ppb). This

510 supports the previous conclusion that although GEOS-CF has a relatively lower biases in the mid-level, the model still struggles  
511 to simulate the extreme O<sub>3</sub> cases. Although GEOS-CF underestimates O<sub>3</sub> magnitude in the HMO cluster, it ~~actually has~~ has a  
512 higher correlation than most of the other clusters (R = 0.51) (Figure 7, Table S1). ~~In comparing the full multi-dimensional lidar~~  
513 ~~and model mean profile curtain (Figure 3),~~ GEOS-CF does a fair job connecting the mid-level higher O<sub>3</sub> pattern in the early  
514 morning that develops down to the low-level later in the afternoon (Figure 3). From this we can draw a conclusion that GEOS-  
515 CF is better able to capture mid-level O<sub>3</sub> patterns earlier in the temporal profile leading to ~~higher~~ better correlations with the  
516 lidar.

517

### 518 ~~3.3.3 Cluster approach and model conclusions~~ Advantages of cluster approach and derived model conclusions

519 ~~Several studies rely on case study investigations or grouping data by altitude to evaluate model performance. As~~  
520 ~~demonstrated in Sect. 3.3.1, we can evaluate the overall summarized the model profile curtains O<sub>3</sub> against the lidar profile~~  
521 ~~curtains and come to the simple conclusion that both models fairly simulate low level O<sub>3</sub> but struggle to simulate mid level~~  
522 ~~O<sub>3</sub>. However, a systematic and comprehensive understanding of the different photochemical regimes in coastal regions does~~  
523 ~~not only require case studies and overall summaries. The clustering approach allows for a comprehensive yet still detailed~~  
524 ~~evaluation of the varying photochemical regimes in coastal regions utilizing the lidar derived full profile curtains. Additionally,~~  
525 ~~using the clusters, we can efficiently evaluate the ability of the models to simulate many different cases of O<sub>3</sub>. This approach~~  
526 ~~revealed specific O<sub>3</sub> cases in which the models perform well and others where the models fail that would have been overlooked~~  
527 ~~by solely considering the overall results. Using the clustering, we are able evaluate how the cluster specific differences (Figure~~  
528 ~~6, Figure 7, and Table S1) reveal additional model performance insight and specific gaps that would be conceivably overlooked~~  
529 ~~when evaluating overall performance.~~

530 It is warranted that models struggle simulating extreme events/cases such as seen in the low-level in the HLO cluster and  
531 in the LLO cluster. However, GEOS-Chem performs best in both clusters with minimal biases and strong to fair correlations.  
532 Our result suggest that GEOS-Chem does a much better job simulating extreme O<sub>3</sub> cases in the low-level than expected. We  
533 can conclude that the non-systemic bias is not only attributed to a good simulation of afternoon O<sub>3</sub> but also a fair simulation  
534 in morning O<sub>3</sub>. Models usually tend to overestimate morning O<sub>3</sub>, but these result reveal GEOS Chem does a better job than  
535 expected. This specific model feature is not eminent when evaluating overall performance. ~~Additionally, overall GEOS Chem~~  
536 ~~performs poorly in the mid-level. The detailed analysis granted by the~~The cluster approach ~~also reveals GEOS Chem has the~~  
537 ~~lowest bias in the LMO cluster signifying the model is better able to capture low O<sub>3</sub> conditions in the mid-level. The overall~~  
538 ~~high systemic positive bias for GEOS-CF in the low-level is further dissected when evaluating the individual clusters. GEOS-~~  
539 ~~CF systematically overestimates low-level O<sub>3</sub>, but the individual clusters indicate that the model has a better correlation with~~  
540 ~~O<sub>3</sub> in the HMO cases cluster. The higher O<sub>3</sub> levels measured throughout the diurnal profile from 1500 – 2000 m are well~~  
541 ~~captured by the model and contribute to the better low-level correlation. An even more profound case is exposed in which~~  
542 ~~GEOS-CF has a strong correlation with mid-level O<sub>3</sub> in the LMO cases despite having a low correlation overall. This concludes~~

543 ~~that in cases where the GEOS-CF model struggles to reproduce O<sub>3</sub> concentrations, the model can still capture the O<sub>3</sub> variability~~  
544 ~~seen by the lidar measurements.~~

545 The clustering approach also reveals more discrepancies in the models such as in the MCO cluster. ~~The advantage of~~  
546 ~~Evaluating the full temporal and vertical profile curtains indicates that we find the~~ overestimation of early morning O<sub>3</sub>  
547 ~~throughout in~~ the low-level ~~leads to the poorer performances in MCO for both models. The overestimation of morning O<sub>3</sub> in~~  
548 GEOS-CF adds to the systemic overestimation in afternoon O<sub>3</sub> contributing the greater bias and poorer correlation. The same  
549 case can be found in the GEOS-Chem MCO cluster performance but to a lesser extent as GEOS-Chem has a much lower  
550 positive bias. Previous studies have found that excessive vertical mixing leads to overestimation of O<sub>3</sub> near the surface as well  
551 as underestimation of O<sub>3</sub> night-time depletion resulting in overestimation of O<sub>3</sub> the next day (Dacic et al., 2020; Keller et al.,  
552 2021; Travis & Jacob, 2019). ~~Model overestimation of O<sub>3</sub> at night and in early morning hours is a common problem for 3-D~~  
553 ~~Eulerian CTMs. Overnight, O<sub>3</sub> concentrations from the evening before can remain lingering in the residual layer. This residual~~  
554 ~~layer sits at about 1000 m or higher depending on the conditions of the environment. O<sub>3</sub> trapped in this residual layer can~~  
555 ~~directly correlate with the next day afternoon O<sub>3</sub> (e.g., Figure 3a; HLO cluster). Models struggle to resolve the shallow surface~~  
556 ~~layer at night, which enhances nighttime NO titration and O<sub>3</sub> dry deposition. If this residual layer and the titration of O<sub>3</sub>~~  
557 ~~overnight in the shallow surface layer is not resolved, next day simulated O<sub>3</sub> will most likely warrant even greater biases. The~~  
558 ~~titration that occurs at night after the initial afternoon build up requires successful simulation to prevent the model beginning~~  
559 ~~the following day with higher O<sub>3</sub> than is observed which can lead to the overprediction of O<sub>3</sub> later that day.~~ Therefore, in the  
560 given case where there is an O<sub>3</sub> event that lasts more than one day (at the same lidar location), the model will likely  
561 underestimate O<sub>3</sub> night-time depletion, overpredict morning O<sub>3</sub>, and subsequently overpredict the afternoon build-up. Given  
562 multiple cases of multi-day ~~or consecutive~~ high O<sub>3</sub> events from the lidar measurements (17 total from HMO, MCO, and HLO),  
563 this is likely one of the reasons for GEOS-CF overestimating early and therefore afternoon O<sub>3</sub> in these high O<sub>3</sub> cases in the  
564 low-level. In Figure 6, GEOS-CF exhibits the greatest afternoon O<sub>3</sub> overprediction in MCO and HLO. In HLO alone, there  
565 were 4 (out of 18) of the profiles that were consecutive while in MCO there were 8 (out of 28). This gives explanation for  
566 upwards of 22 – 29 % of the overestimation of O<sub>3</sub> in the profile curtains of these clusters. These multi-day O<sub>3</sub> events are  
567 particularly important as they can indubitably lead ~~the models to~~ ~~higher overprediction overestimations~~ of afternoon O<sub>3</sub>. ~~As the~~  
568 ~~full lidar profile curtains reveal, the models tend to overestimate early morning O<sub>3</sub> in the MCO cases which links to the~~  
569 ~~overestimation in afternoon O<sub>3</sub> as well.~~ Full vertical and temporal curtains provided by lidar instruments are essential in fully  
570 ~~understanding the development and depletion of O<sub>3</sub> in these cases. The mean curtain profiles in Figure 3a indicate that what is~~  
571 ~~captured at the surface (below 500 m) in the early morning does not represent what is captured in the residual layer (1000 m)~~  
572 ~~by the lidar. Therefore, surface data would not be sufficient in evaluating a multi-day event.~~

573  
574 ~~GEOS-Chem does not have such an issue overestimating low-level O<sub>3</sub> in the afternoon. In the other clusters, GEOS-~~  
575 ~~Chem actually underpredicts early morning low-level O<sub>3</sub> in the full vertical profile and does an overall better job than GEOS-~~  
576 ~~CF simulating morning low-level O<sub>3</sub>, such as in the HLO cluster. A better estimation of early morning O<sub>3</sub> does not warrant the~~

577 ~~same build-up of afternoon O<sub>3</sub>. In these cases, GEOS-Chem handles the multi-day simulations better than GEOS-CF. This~~  
578 ~~gives some explanation to why GEOS-Chem underpredicts the other clusters with higher O<sub>3</sub> concentrations in the low-level~~  
579 ~~(HMO and HLO). Both models have a better ability to simulate early morning O<sub>3</sub> magnitude and pattern for other clusters than~~  
580 ~~the MCO. For example, GEOS-CF does best simulating morning low-level O<sub>3</sub> in cases of lower O<sub>3</sub> extent (LLO and LMO),~~  
581 ~~but still overestimates the afternoon O<sub>3</sub>. Since in these cases the afternoon does not seem to be related to early morning~~  
582 ~~overestimations, other factors may be contributing. In the LLO cluster, the full curtain profile implies excessive mixing~~  
583 ~~throughout the entire vertical profile could be adding to afternoon O<sub>3</sub> overestimation. Similarly, for the LMO cluster, mid-~~  
584 ~~level O<sub>3</sub> seems to be at play in influencing low-level O<sub>3</sub> which could be adding to afternoon biases. GEOS-Chem does not~~  
585 ~~have such an issue overestimating low-level O<sub>3</sub> in the afternoon. In the other clusters, GEOS-Chem actually underpredicts~~  
586 ~~early morning low-level O<sub>3</sub> in the full vertical profile. An underestimation of early morning O<sub>3</sub> does not warrant the same~~  
587 ~~build-up of afternoon O<sub>3</sub>. This gives some explanation to why GEOS-Chem underpredicts the other clusters with higher O<sub>3</sub>~~  
588 ~~concentrations in the low-level (HMO and HLO).~~

589 In the mid-level GEOS-Chem ~~has a systemic high negative bias for all clusters,~~ consistently underestimates ~~ing~~ O<sub>3</sub> but  
590 the clusters reveal a better performance in LMO, ~~the cluster with lowest mid-level O<sub>3</sub> extent.~~ It is evident that the model is  
591 ~~better able to capture lower magnitude O<sub>3</sub> cases in the mid-level. A unique case is exposed in which GEOS-CF has a strong~~  
592 ~~correlation in the mid-level in the LMO cluster despite having a low correlation overall and in the other clusters. The individual~~  
593 ~~cluster correlation reveals the GEOS-CF model is better able to capture the higher O<sub>3</sub> observations in this cluster thus capturing~~  
594 ~~more of the variability. It is evident that the model cannot simulate cases with higher O<sub>3</sub> concentrations in the mid-level but~~  
595 ~~simulates low O<sub>3</sub> cases better. On the other hand, GEOS-CF results indicate a lower non-systemic bias in the mid-level.~~ Since  
596 the version of GEOS-Chem used in this study was run with the tropchem chemistry mechanism which excludes stratospheric  
597 chemistry (now obsolete with current GEOS-Chem developments) and GEOS-CF uses the UCX chemistry mechanism that  
598 includes stratospheric chemistry, this may allude to better performance of GEOS-CF in simulating higher O<sub>3</sub> concentrations in  
599 the mid-level. ~~The weak correlations in the mid-level could be due to multiple model inefficiencies such as the coarse model~~  
600 ~~resolutions. Both models indicate weak correlations with the lidar observations in the mid-level and it is apparent that both~~  
601 ~~models struggle to capture the pattern of O<sub>3</sub> behavior in the mid-level. This could be due to multiple model inefficiencies such~~  
602 ~~as the coarse model resolutions.~~ Although GEOS-CF has a finer resolution than GEOS-Chem, it still may not be sufficient in  
603 horizontal and vertical grid resolution to replicate the O<sub>3</sub> variations captured in the 2-D lidar observations. ~~Additionally,~~  
604 ~~transport of emissions in the free troposphere (FT) is another influential factor that could contribute to the misrepresentation~~  
605 ~~of mid-level O<sub>3</sub>. In Figure S8, aircraft measurements from OWLETS-2 are used to evaluate GEOS-Chem simulated carbon~~  
606 ~~monoxide (CO) in the FT (1800 – 2500 m AGL). The flight days evaluated are all curtain profiles that were assigned to the~~  
607 ~~clusters with higher levels of O<sub>3</sub> in the mid-level (HMO, MCO, and HLO). It is evident that the model is able to capture lower~~  
608 ~~levels of CO in the FT (100 – 110 ppbv) (e.g., background levels) but struggles to capture the higher levels (130 – 140 ppbv).~~  
609 ~~Since increased levels of CO in the FT are indicative of possible long-range transport (Neuman et al., 2012), FT transport~~  
610 ~~could be a factor contributing to the GEOS-Chem poor performance in the mid-level.~~



611 There are additional model discrepancies that can lead to underestimations of O<sub>3</sub> in GEOS-Chem in the mid-level that  
612 was found in all 5 clusters. One gap in the GEOS-Chem model could be the representation of tropospheric halogen chemistry  
613 which has a large effect of coastal O<sub>3</sub> production. Newer updates to the GEOS-Chem model (v12.9) have included updated  
614 tropospheric halogen chemistry mechanisms (iodine, bromine, and chlorine) (Wang et al., 2021) ~~and indicate~~ ~~This study~~  
615 ~~found that the updated halogen chemistry actually worsens the overall underestimation of O<sub>3</sub> throughout the troposphere,~~  
616 ~~specifically in the northern hemisphere, indicating~~ further investigation of halogen chemistry is needed for better model  
617 representation. Another study finds a similar conclusion in the proper representation of cloud uptake and tropospheric  
618 chemistry ~~in the model~~ (Holmes et al., 2019). ~~This study found that implementing an updated, more accurate, and stable cloud~~  
619 ~~entrainment limited uptake in the GEOS-Chem model reduces the sensitivity of oxidants and aerosol chemistry in the~~  
620 ~~troposphere but still had little effect on O<sub>3</sub> model comparison to observations (such as sonde and aircraft). This is due to the~~  
621 ~~environmental variability being much higher than the effect of NO<sub>x</sub> and O<sub>3</sub> cloud chemistry but still~~ warranting further testing.  
622 The role lightning plays in tropospheric oxidation is another feature that is commonly misrepresented in global models and  
623 can affect O<sub>3</sub> simulation (Mao et al., 2021). These are all examples of features that if not simulated correctly can lead to  
624 misestimations of O<sub>3</sub>. The clustering approach allows us to organize the detailed lidar measurements to scope out specific  
625 cases where these misrepresentations occur. These previous studies also highlight the importance of lidar measurements and  
626 their ability to depict tropospheric emission development and behavior throughout the vertical profile and diurnal cycle which  
627 can be used to constrain model emissions and improve simulations.

628 Although this analysis proves to be a useful technique to characterize the largely variably O<sub>3</sub> behavior in coastal regions  
629 and evaluate the subsequent model performance, there are also limitations. In this study we are comparing single point lidar  
630 versus model output, therefore we cannot simply state that the model is incorrect. We make conclusions and draw biases based  
631 on the ability to subset a grid point and compare that to a single point lidar curtain to the best ability but that still leaves an  
632 uncertainty. ~~The high vertical and spatiotemporal resolution reveal intricate details about the behavior of O<sub>3</sub> during these~~  
633 ~~campaigns. O<sub>3</sub> lidars have a unique advantage, compared to traditional surface measurements, in measuring vertical~~  
634 ~~distribution of O<sub>3</sub> with respect to time. This advantage is of great value when investigating model ability in simulating the~~  
635 ~~spatial and temporal distribution of O<sub>3</sub> and can provide crucial information in understanding surface O<sub>3</sub> events.~~

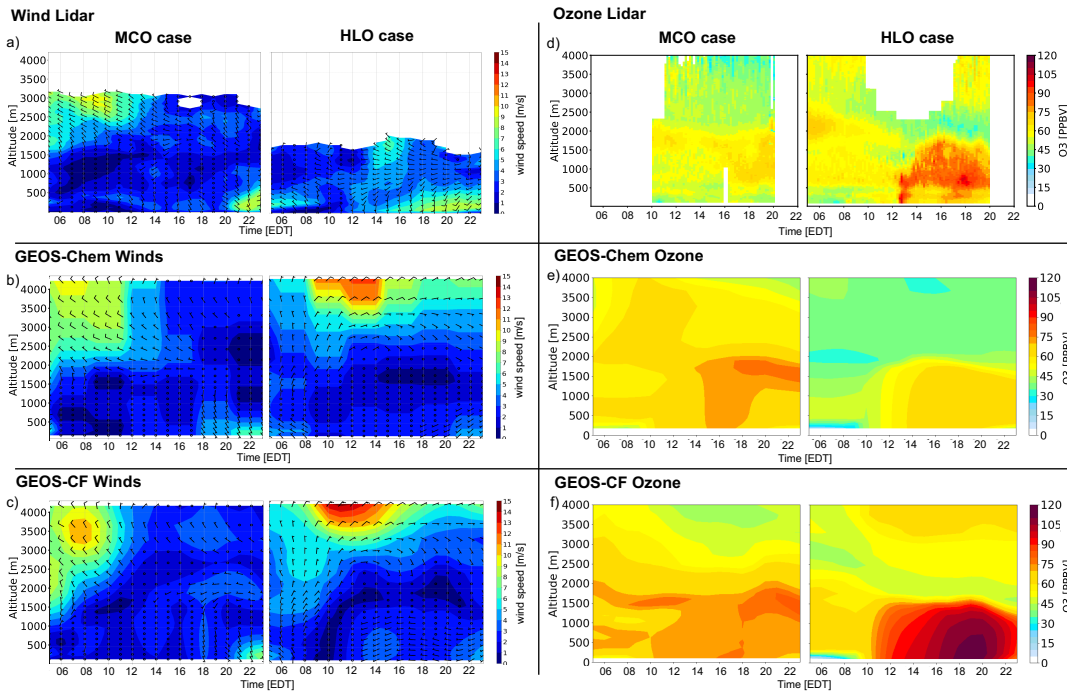
636

### 637 **3.4 Cluster derived case studies to evaluate modeled wind and ozone**

638 Meteorological factors such as wind speed and direction can directly impact whether a coastal region will experience  
639 clean air or O<sub>3</sub> exceedances. When local meteorological processes such as sea/bay breeze occur at such a fine scale, equally  
640 fine resolution measurements are essential in capturing this. The Doppler wind lidar offers a focus on fine details that are only  
641 revealed in the multi-dimensional data which allows for such a comprehensive evaluation of the established O<sub>3</sub> cluster profile  
642 curtains. In this sect., we evaluate the 2-D relationship between wind and O<sub>3</sub> to assess model performance using lidar and  
643 model derived profile curtains (Figure 8). We derived two specific case studies, each from a different cluster: MCO = 17 June  
644 2018 and HLO = 30 June 2018. Utilizing the derived clusters, the case studies were chosen to focus on high low-level O<sub>3</sub>



645 behavior cases with a goal of evaluating possible sea/bay breeze events. The two case studies are both from the HMI location  
 646 during the OWLETS-2 campaign. ~~There are consistent Doppler lidar measurements throughout the low-level (<2000 m) which~~  
 647 ~~allows for a direct comparison with the simulated profiles; therefore, the focus of the following analysis will be on the low-~~  
 648 ~~level altitudes. The deficit of mid level observed wind data disallows for a conclusive and concrete evaluation of simulated~~  
 649 ~~mid level O<sub>3</sub>. The white spaces in both the wind and O<sub>3</sub> lidar indicate missing data.~~  
 650



651  
 652 Figure 8. Profile curtains of wind speed/direction (a-c) and ozone (d-f) from the lidar (top panel), GEOS-Chem (middle panel),  
 653 and GEOS-CF (bottom panel). Results from OWLETS-2 at HMI. Wind direction is depicted by wind barbs. The white spaces  
 654 indicate missing data for both the a) wind and d) lidar curtain profiles.

655 ~~Figure 8. Profile curtains of wind speed/direction (a-c) and ozone (d-f) from the lidar (top panel), GEOS-Chem (middle panel),~~  
 656 ~~and GEOS-CF (bottom panel). Results from OWLETS-2 at HMI.~~

657

### 658 3.4.1 Sea breeze event interpretation

659 ~~GEOS-Chem and GEOS-CF both struggle to capture low-level wind speed and direction in both MCO and HLO cases~~  
 660 ~~(Figure 8a-c).~~ In the MCO case, the Doppler wind lidar captures a wind direction shift from westerly to easterly winds  
 661 beginning at 06:00 EDT accompanied by calm winds (approximately  $0 \text{ m s}^{-1}$ ) indicating an early onset sea/bay breeze event.  
 662 The timing of the start of this event is simulated well but the models fail to predict an actual well-defined wind shift, instead  
 663 merely simulating  $0 \text{ m s}^{-1}$  winds after 05:00 EDT. ~~It is apparent that the models struggle to capture the finer processes such as~~

664 ~~a sea/bay breeze which could have likely led the underprediction of wind speed. It is important to note that GEOS-Chem runs~~  
665 ~~with offline meteorology, averaged every 3 hours. Since sea/bay breezes often happen at a finer temporal resolution, the GEOS-~~  
666 ~~Chem model is at a disadvantage in modeling such fine processes.~~ A wind direction shift is ~~also~~ depicted in the HLO case,  
667 with westerly winds early in the morning and a shift to south-easterly winds later in the temporal profile (at about 10:00 EDT).  
668 This could also likely be a common sea breeze event which could have contributed to the high observed O<sub>3</sub> concentrations in  
669 the afternoon. Again, the exact timing of the start of the wind shift is captured by the models but then no defined directional  
670 shift and little to no winds are simulated after with a worse performance for the GEOS-Chem model. ~~Both the MCO case and~~  
671 ~~HLO case observe increased wind speeds near the surface, first before 08:00 EDT then again in the evening. Both models~~  
672 ~~underestimate the extent of the increased wind speeds.~~ Based on the Doppler wind lidar curtain profiles, we can derive that the  
673 two sea/bay breeze cases are distinct. The HLO case closely mirrors a common sea/bay breeze event with a more definite wind  
674 direction shift later in the morning and winds above the surface remain consistent throughout the profile. The MCO case shows  
675 a less discernible wind shift which also begins earlier in the morning with weaker winds above the surface. These differences  
676 are not well captured by either model. It is important to note that GEOS-Chem runs with offline meteorology, averaged every  
677 3 hours. Since sea/bay breezes often happen at a finer temporal resolution, the GEOS-Chem model is at a disadvantage in  
678 modeling such fine processes.

679

#### 680 **3.4.2 Wind relation to ozone cases and clustering**

681 In this sect., the wind lidar curtains will be assessed in relation to the O<sub>3</sub> lidar profile curtains and the model performance.  
682 ~~We show in sect. 3.3.2 that, both models have the highest bias and lowest correlation simulating low-level O<sub>3</sub> in the MCO~~  
683 ~~cluster. The results in sect. 3 revealed that both models had the highest bias and lowest correlation simulating low level O<sub>3</sub> in~~  
684 ~~MCO. Mirroring those results, both models overestimate low-level O<sub>3</sub> in the MCO case studies (Figure 8e, f). Evaluating the~~  
685 ~~wind and O<sub>3</sub> lidar profile curtains against the model simulations helps paint a better picture as to why. Similar to the MCO~~  
686 ~~cluster mean curtain profile, early morning low level O<sub>3</sub> in each case is overestimated by both models (Figure 8e, f). Higher~~  
687 ~~O<sub>3</sub> concentrations are captured in the lidar curtain profile throughout the day, but is constrained between 1000 – 2000 m. Both~~  
688 ~~models bring this high O<sub>3</sub> pattern down to the surface (below 500 m) which contributes to the overestimation. The models~~  
689 ~~predict little to no winds in the low-level simulating a stagnant environment. Simulated stagnant winds reflect lower dilution~~  
690 ~~rates and induce higher O<sub>3</sub> concentration build-up near the surface that is reproduced in both models. For the mid-level, the~~  
691 ~~GEOS-CF model seems to replicate O<sub>3</sub> pattern better, while GEOS-Chem overestimates O<sub>3</sub>. This is a unique finding that was~~  
692 ~~not detected in the previous analysis where GEOS-Chem was found to consistently underestimate mid-level O<sub>3</sub>. From the data~~  
693 ~~available above 2000 m, both models seem to do well replicating mid-level winds. This implies that there are more factors at~~  
694 ~~play such as transport or background level O<sub>3</sub> that may have prompted the overestimated O<sub>3</sub> in these cases. There is higher O<sub>3</sub>~~  
695 ~~captured in the lidar curtain profile, but it is constrained between 1000 – 2000 m. Both models bring this higher O<sub>3</sub> pattern~~  
696 ~~down to the surface (below 500 m) overestimating O<sub>3</sub> throughout the low level. Since both models predict little to no winds~~  
697 ~~during this time, this could contribute to overestimations of O<sub>3</sub> near the surface.~~

698 ~~In the HLO case, GEOS-CF overestimates low-level O<sub>3</sub> while GEOS-Chem underestimates low-level O<sub>3</sub>.~~  
699 ~~For the HLO cluster, GEOS-CF had a high positive mean normalized bias and a reasonable relationship (R = 0.61) in the~~  
700 ~~low-level (sect. 3). From sect. 3.3 the results revealed that although GEOS-CF has a high positive normalized bias for low-~~  
701 ~~level O<sub>3</sub> in HLO, the model had a reasonable relationship (R = 0.61) with the O<sub>3</sub> lidar measurements. This is corroborated. For~~  
702 ~~the individual HLO case (Figure 8f), GEOS-CF was similarly found to overestimate low-level O<sub>3</sub> magnitude while better able~~  
703 ~~to capture the O<sub>3</sub> pattern. GEOS-CF is better able to reproduce the wind shift in HLO (Figure 8c) but, like the MCO case,~~  
704 ~~stagnant winds simulated earlier in the morning suggest a similar overestimation of early morning O<sub>3</sub>. This is another clear~~  
705 ~~example supporting the tendency for GEOS-CF to overestimate morning O<sub>3</sub> which can facilitate an overestimation in the~~  
706 ~~afternoon. The GEOS-Chem HLO case results mirror its mean cluster performance closely by underestimating both low-level~~  
707 ~~and mid-level O<sub>3</sub>. For this case, the simulated winds indicate a very different result than the lidar winds, simulating no winds~~  
708 ~~in the low-level for almost the entirety of the temporal profile and vertical profile. Since the results reveal O<sub>3</sub> is underestimated,~~  
709 ~~this suggests that there are more factors affecting O<sub>3</sub> results in this specific case. One of these factors can be the simulation of~~  
710 ~~the boundary layer as the sea/bay breeze develops. If the boundary layer is simulated to be larger in depth, the ability for the~~  
711 ~~model to simulate higher O<sub>3</sub> concentrations may be hindered such as found in Dacic et al. (2017). Since the HLO case indicates~~  
712 ~~a common sea breeze event based on the timing and shift, it appears that GEOS-Chem really struggles capturing this intricate~~  
713 ~~process while GEOS-CF does a better job. with the individual HLO case (Figure 8f) as GEOS-CF is better able to simulate the~~  
714 ~~development of O<sub>3</sub> in the low-level, especially in the early morning. The GEOS-CF modeled winds mirror this performance~~  
715 ~~with a better reproduction of the wind shift in HLO (Figure 8c). While GEOS-Chem has a lower normalized bias for low-level~~  
716 ~~O<sub>3</sub> in the HLO cluster, GEOS-Chem consistently underestimates wind speed and fails to reproduce any wind shifts. This reveals~~  
717 ~~that in the possible sea breeze event, the two models do not perform equally. Since GEOS-Chem is an offline CTM using~~  
718 ~~archived meteorology and GEOS-CF simulates atmospheric composition simultaneously with meteorology (online), the~~  
719 ~~replication of a sea breeze case would not necessarily be comparable.~~

720 ~~It is evident from these cases that differences in sea/bay breeze events can lead to diverse O<sub>3</sub> profiles. The HLO case high~~  
721 ~~O<sub>3</sub> levels that reach down to the surface, with peaks > 75 ppb at both 12:00 and again at 16:00 EDT. Just above this extreme~~  
722 ~~O<sub>3</sub> plume at 2000 m, there is an O<sub>3</sub> deficit of almost 50 ppb. The MCO case differs in that the highest O<sub>3</sub> concentrations do not~~  
723 ~~reach the surface. Also, O<sub>3</sub> is more distributed and mixed throughout the curtain profile and the vertical gradient, although~~  
724 ~~present, is not as stark as the HLO case. The HLO cases also has higher O<sub>3</sub> captured aloft above 2500 m which is not captured~~  
725 ~~in the MCO case. Analyzing their full curtain profiles, it is easy to conclude why these events were not assigned to the same~~  
726 ~~cluster and the differences are also apparent in the individual model performance. For both cases, the models generally seem~~  
727 ~~to underestimate wind speed and overestimate O<sub>3</sub> (to different extents) but the GEOS-Chem performance in the HLO case is~~  
728 ~~different. The uniqueness of this case implies that GEOS-Chem struggles to simulate this sea/bay breeze based on factors other~~  
729 ~~than wind speed and direction.~~

730 ~~In most cases, sea/bay breeze events can contribute to high concentrated daytime O<sub>3</sub> events in which O<sub>3</sub> is recirculated~~  
731 ~~throughout the region. Such cases would likely lead to a similar curtain profile as seen in the HLO case (Figure 8a), where~~

732 ~~high  $O_3$  in the morning is likely associated with the higher  $O_3$  at the surface in the afternoon. But it is apparent that the cases~~  
733 ~~for MCO and HLO are dissimilar. We would expect per the clustering approach that sea breeze cases would most likely be~~  
734 ~~assigned to the same cluster, but this is not the case here. Investigating the full lidar and model profile curtains for the two~~  
735 ~~cases gives us more information as to why these two curtains are not in the same cluster. It is evident that the HLO case has~~  
736 ~~much higher afternoon  $O_3$  near the surface (below 1000 m) than the MCO case, with peaks  $> 75$  ppb at both 12:00 and again~~  
737 ~~at 16:00 EDT. In contrast, the MCO case has higher afternoon  $O_3$  concentrations captured above 2000 m than the HLO case.~~  
738 ~~The HLO case has high  $O_3$  in the afternoon, but it is constrained to the lower 2000 m and just above this high  $O_3$  plume, there~~  
739 ~~is an  $O_3$  deficit of almost 50 ppb. Although the MCO case also reveals lower  $O_3$  above 2000 m, the vertical gradient in this~~  
740 ~~case is not as stark. This is also replicated in both models which simulate lower  $O_3$  directly above the high surface  $O_3$  in the~~  
741 ~~HLO cluster but simulate higher  $O_3$  above 2000 m in the MCO cluster. From their distinct vertical and temporal behavior, it~~  
742 ~~is easy to conclude why these two cases were not assigned to the same cluster.~~

743 It is imperative to correctly simulate coastal mechanisms in order to mitigate high  $O_3$  events. ~~The cases elected for MCO and~~  
744 ~~HLO give reason to address the difficulty simulating complex coastal mechanisms. Despite the fact that MCO and HLO both~~  
745 ~~indicated prospective sea/bay breeze cases, the results of the simulated winds and  $O_3$  were distinctive. Simulating complex~~  
746 ~~sea/bay and land relations is imperative for correctly mitigating high  $O_3$  cases.~~ To accurately simulate such complex exchanges,  
747 high resolution vertical and horizontal simulations are needed. Because of the models' relatively coarse resolutions (nominally  
748 50 and 25 km horizontal resolution; 72 vertical levels), the fine-scale vertical wind gradients and horizontal wind shifts are  
749 difficult to resolve and, in these cases, not fully able to replicate. This study also acknowledges the need for an evaluation of  
750 other modeled factors, aside from model resolution, such as divulged in sect. 3.3.3, considering the possible confounding  
751 effects on modeled  $O_3$  outcome.

#### 755 4. Conclusion

756 We developed ~~and tested~~ a clustering method based on a suite of 91 multi-dimensional lidar  $O_3$  profile curtains  
757 retrieved from three recent ~~land/sea~~ campaigns (~~OWLETS 1, OWLETS 2, and LISTOS~~), ~~during the summer months of 2017~~  
758 ~~and 2018~~. The K-Means clustering algorithm, driven by 8 well defined features, was applied to categorize the fine resolution  
759  $O_3$  data, revealing five distinct  $O_3$  behavior cases that are distinct all vary in pattern and magnitude vertically and temporally.  
760 ~~We present five different clusters of  $O_3$  behavior identified as: highest mid-level  $O_3$  (HMO) cluster; lowest low-level  $O_3$  (LLO)~~  
761 ~~cluster; most common  $O_3$  (MCO) cluster; highest low-level  $O_3$  (HLO); lowest mid-level  $O_3$  (LMO) cluster.~~ The results indicate  
762 that fine resolution data can be used to characterize highly variable vertical and temporal coastal  $O_3$  behavior and classify  
763 different cases of  $O_3$  exploiting the multiple dimensions. ~~The results indicate that fine resolution data can be used to~~  
764 ~~differentiate the behavior of  $O_3$  in a region and classify different cases of  $O_3$  exploiting the multiple dimensions. The clustering~~  
765 ~~approach allowed us to characterize the range of highly variable vertical and temporal coastal  $O_3$  behavior for the duration of~~

766 ~~these campaigns which can be a good indicator of how O<sub>3</sub> behaves in general in these coastal regions during the summer~~  
767 ~~months.~~ Furthermore, this approach could be used by states to better identify different O<sub>3</sub> photochemical regimes and frequency  
768 beyond just surface sampling.

769 ~~We evaluated the~~The performance of two CTMs (GEOS-Chem and GEOS-CF) were evaluated, ~~GEOS-Chem and~~  
770 ~~GEOS-CF.~~ Overall, the models ~~have the greatest difficulty simulating the vertical extent and variability of O<sub>3</sub> concentrations~~  
771 ~~in the mid-level, had a with~~ weak overall relationships ~~to with~~ the lidar observations in the mid-level (R = 0.12 and 0.22).  
772 GEOS-Chem had a systematic high negative bias and GEOS-CF had an overall lower unsystematic bias range. In the low-  
773 level, GEOS-Chem had overall low unsystematic bias range and fair relationship with the lidar observations (R = 0.66), while  
774 GEOS-CF had a systematic high positive bias but overall fair relationship (R = 0.69).

775 Utilizing the curated clusters reveals new model insight that is neglected in the overall performance analysis. ~~The~~  
776 ~~cluster approach divulges specific model limitations but also cases in which the models perform well.~~ GEOS-Chem simulates  
777 ~~low level O<sub>3</sub> cases best in the HLO and LLO clusters and the worst in the MCO cluster. HLO and LLO are the clusters with~~  
778 ~~the most extreme (low and high) O<sub>3</sub> cases while MCO is the most common cluster with moderate O<sub>3</sub>. This concludes that~~  
779 ~~GEOS-Chem does best simulating extreme O<sub>3</sub> cases in the low-level O<sub>3</sub> (such as in HLO and LLO) but struggles to capture the~~  
780 ~~frequently occurring moderate O<sub>3</sub> behavior. The greater underestimations of mid-level O<sub>3</sub> for GEOS-Chem can be alluded to~~  
781 ~~multiple model discrepancies such as the mechanism used (tropchem) which only considers tropospheric chemistry. Another~~  
782 ~~factor inhibiting the poor simulation in the mid-level is the model failing to capture long-range transport of emissions in the~~  
783 ~~FT. GEOS-CF also has the greatest overestimations for low level O<sub>3</sub> in the MCO cluster.~~ Evaluating the full profile curtains  
784 reveals that ~~this GEOS-CF low-level~~ overestimations can be most attributed to the greater overestimation of early morning O<sub>3</sub>.  
785 This feature is ~~unique to the MCO cluster~~ affiliated to multi-day O<sub>3</sub> events and warrants further investigation as where O<sub>3</sub> left  
786 lingering in the residual layer overnight can contribute to higher O<sub>3</sub> in the afternoon the next day and proves to be a challenge  
787 for CTMs. Lidar curtain profiles prove to be essential in evaluating these multi-day cases as they can capture the full  
788 development and deposition of O<sub>3</sub> in the residual layer that is not observed at the surface. The value of lidar measurements is  
789 reflected in its ability to reveal these features.

790 ~~Both models share poor performances in the mid level but there are specific cases that stand out in the clustering~~  
791 ~~results, specifically the LMO cluster, in which GEOS-CF shares a good agreement with the lidar measurements. It can be~~  
792 ~~concluded that~~ Although ~~the~~ we find the GEOS-CF model struggles to simulate O<sub>3</sub> magnitude in the mid-level, it can relatively  
793 emulate ~~the mid-level O<sub>3</sub> pattern variability in LMO~~ some cases (LMO cluster). GEOS-CF also does fairly well in cases in  
794 which the pattern of higher mid-level O<sub>3</sub> suggests a relationship with the low-level O<sub>3</sub>. This is also apparent in the MCO cluster,  
795 in which the pattern of higher mid-level O<sub>3</sub> that suggests a relationship with the low-level O<sub>3</sub> is simulated fairly in the GEOS-  
796 CF model. This pattern is also a rare feature that is captured in the lidar that demonstrates the significance of the measurements.  
797 ~~The greater underestimations of mid-level O<sub>3</sub> for GEOS-Chem can be alluded to multiple model discrepancies. Since the~~  
798 ~~GEOS-Chem version and mechanism used in this study (tropchem) only considers tropospheric chemistry we can expect the~~  
799 ~~performance in the mid-level to have deficiencies.~~ Although GEOS-CF is run with the combined tropospheric and stratospheric

800 chemistry mechanism, has a ~~better~~finer grid resolution, and is an online model, we conclude there are still limitations to both  
801 models ~~especially when simulating mid-level O<sub>3</sub>. Known model errors and coarse horizontal and vertical grid resolution~~which  
802 ~~contribute to the difficulty in simulating fine-scale coastal O<sub>3</sub> variability. There are many contributing model factors that can~~  
803 ~~be affecting the performance of GEOS-Chem and GEOS-CF that were mentioned in this study not solely coarse model~~  
804 ~~resolution.~~

805 We demonstrate a unique value of the clustering approach on multi-dimensional lidar data ~~is that it offers a~~  
806 ~~convenient way to ascertain different O<sub>3</sub> case studies. An example of this is our n~~ which we use the cluster results to evaluate  
807 ~~of two cases studies from the MCO and HLO clusters. Modeled winds were evaluated using Doppler wind lidar data observed~~  
808 ~~during the OWLETS-2 campaign. The wind lidar data was mostly limited to lower altitudes (< 2000 m), which allowed for~~  
809 ~~wind speed and direction validation at the low level. The morning wind deceleration speed~~ and directional shifts (onshore to  
810 offshore) illustrated in wind lidar profile curtains indicate a possible sea/bay breeze event in both case studies. The two cases  
811 represent distinct sea/bay breeze events that lead to different O<sub>3</sub> developments that were difficult for the CTMs to reproduce.  
812 ~~This is likely another contributor that led to enhanced surface O<sub>3</sub> in these cases. Due to the coarse~~ model resolution and other  
813 possible factors, GEOS-Chem and GEOS-CF were not able to capture the sea breeze phenomena in these cases which could  
814 ~~have facilitated in the high O<sub>3</sub> biases for these clusters. With GEOS-CF having a finer horizontal resolution than GEOS-Chem,~~  
815 ~~the results reveal minimal advantages simulating the pattern of wind speeds better but none in simulating the wind directional~~  
816 ~~shifts. This affirms that the spatial resolution of GEOS-CF (~25 km) is still not fine enough for mesoscale processes such as~~  
817 ~~the sea/bay breeze. Although~~ With a regional model analysis ~~is being~~ out of the scope of this study, we propose to use multi-  
818 dimensional lidar measurements to evaluate finer regional modeling in our future work. ~~We acknowledge that other factors,~~  
819 ~~aside from model resolution, contribute to discrepancies in modeled coastal O<sub>3</sub> and further warrant a deeper evaluation. The~~  
820 ~~clustering approach on lidar measurements offers an unmatched ability to pinpoint these features.~~

821 This work is the first time that all three associated campaign lidar data have been analyzed in conjunction. ~~In utilizing~~  
822 ~~the highly detailed suite of multi-dimensional lidar data, we are able to comprehensively explore the behavior and variability~~  
823 ~~of coastal O<sub>3</sub> for the duration of the campaigns. The value of lidar measurements is reflected in its ability to reveal unique~~  
824 features within the temporal and vertical pattern of O<sub>3</sub> behavior. Applying the clustering analysis directly to the lidar O<sub>3</sub> data  
825 emerges as a useful and robust approach for identifying O<sub>3</sub> ~~patterns~~regimes ~~during the highly polluted summer months in~~  
826 ~~coastal environments. Since the time of the OWLETS and LISTOS campaigns, the lidar instrument systems have been updated~~  
827 ~~and are now more fully automatized for use eliminating such constraints faced in this study.~~ Further observations using lidar  
828 instruments should be especially valuable in investigating coastal O<sub>3</sub> behavior as it can divulge the finer-scale O<sub>3</sub> characteristics  
829 that remain difficult to successfully simulate in CTMs. ~~The time-height and fine resolution measurements only available from~~  
830 ~~multi-dimensional lidar instruments were vital in allowing us to form these conclusions.~~

831 ~~This kind of evaluation allows for detailed model assessment of specific O<sub>3</sub> cases that are unmasked through the~~  
832 ~~clustering analysis. Looking at the overall correlations, it would seem the models have a good relationship with the low level~~  
833 ~~lidar observations but looking into the cluster by cluster differences, the gaps within the models are elucidated. Using the~~



834 ~~cluster assignments, we are able to evaluate how the cluster-specific differences reveal additional model performance insight that~~  
835 ~~could be conceivably overlooked when evaluating overall performance.~~ We provide a new approach that is the middle ground  
836 between looking at specific cases and summarizing overall model performance that allows a synopsis of summer coastal O<sub>3</sub>  
837 behavior and subsequently model performance without completely muting distinct O<sub>3</sub> features. ~~This work is a middle ground~~  
838 ~~between looking at specific cases (or dates) and summarizing overall model performance. Additionally, the clustering approach~~  
839 ~~provides an abridged way to detecting distinctive case studies.~~ We provide a new approach that allows a synopsis of summer  
840 coastal O<sub>3</sub> behavior and subsequently model performance without completely muting distinct O<sub>3</sub> features. Evaluating model  
841 performance for diverse O<sub>3</sub> behavior in coastal regions is crucial for improving the simulation and furthermore, mitigation of  
842 air quality events.

843 *Code availability.* Model code is available upon request to the first author.

844 *Data availability.* The GEOS-Chem model simulation data from this study is publicly accessible online at  
845 <https://doi.org/10.7910/DVN/V99LHT>. The GEOS-CF model data is publicly available online at their website  
846 [https://gmao.gsfc.nasa.gov/-weather\\_prediction/GEOS-CF/](https://gmao.gsfc.nasa.gov/-weather_prediction/GEOS-CF/). The lidar data is publicly available online at [https://www-](https://www-air.larc.nasa.gov/missions.htm)  
847 [air.larc.nasa.gov/missions.htm](https://www-air.larc.nasa.gov/missions.htm).

848 *Supplement.*

849 *Author contributions.* CB and YW conceived the research idea. CB wrote the initial draft of the paper and performed the  
850 analyses and model development. All authors contributed to the interpretation of the results and the preparation of the paper.

851 *Competing interests.* The authors declare that they have no conflict of interest.

852 *Acknowledgements.* This study is supported by NASA MUREP Graduate Fellowship (80NSSC19K1680). The Ozone Water-  
853 Land Environmental Transition Study (OWLETS-1, 2) and Long Island Sound Tropospheric Ozone Study (LISTOS) field  
854 measurements described here were funded by the NASA's Tropospheric Composition Program and Science Innovation Fund  
855 (SIF), Maryland Department of Environment, the National Oceanic and Atmospheric Administration (NOAA), the  
856 Environmental Protection Agency (EPA), the Northeast States for Coordinated Air Use Management (NESCAUM), and the  
857 New Jersey and Connecticut Departments of Energy and Environmental Protection. The authors acknowledge the principal  
858 investigators and data operators John Sullivan, Joel Dreessen, Ruben Delgado, William Carrion, and Joseph Sparrow as well  
859 as the guidance of the Tropospheric Ozone Lidar Network (TOLNet). LMOL and TROPOZ data are publicly available at  
860 (<https://www-air.larc.nasa.gov/missions/TOLNet/>). The OWLETS and LISTOS data are available at ([https://www-](https://www-air.larc.nasa.gov/)  
861 [air.larc.nasa.gov/](https://www-air.larc.nasa.gov/)). The Doppler wind data taken from the UMBC wind lidar and are publicly available at ([https://www-](https://www-air.larc.nasa.gov/cgi-bin/ArcView/owlets.2018)  
862 [air.larc.nasa.gov/cgi-bin/ArcView/owlets.2018](https://www-air.larc.nasa.gov/cgi-bin/ArcView/owlets.2018)). ~~The aircraft measurements from the UMD Cessna 402B Research Aircraft~~



863 are publicly available at (<https://www-air.larc.nasa.gov/cgi-bin/ArcView/owlets.20180>). The GEOS-CF model simulation data  
864 were provided directly from the NASA Center Global Modeling and Assimilation Office (GMAO) at the Goddard Space Flight  
865 Center ([https://gmao.gsfc.nasa.gov/weather\\_prediction/GEOS-CF/](https://gmao.gsfc.nasa.gov/weather_prediction/GEOS-CF/)).

## 866 References

867 Alonso, A. M., Berrendero, J. R., Hernández, A., and Justel, A.: Time Series Clustering Based on Forecast Densities,  
868 Computational Statistics & Data Analysis, 51(2), 762–776., <https://doi.org/10.1016/j.csda.2006.04.035>, 2006.

869 Banta, R. M., Senff, C. J., Nielsen-Gammon, J., Darby, L. S., Ryerson, T. B., Alvarez, R. J., Sandberg, S. P., Williams, E. J.,  
870 and Trainer, M: A bad air day in Houston. Bulletin of the American Meteorological Society, 86(5), 657–  
871 670. <https://doi.org/10.1175/BAMS-86-5-657>, 2005.

872 Bernier, C., Wang, Y., Estes, M., Lei, R., Jia, B., Wang, S., and Sun, J.: Clustering Surface Ozone Diurnal Cycles to Understand  
873 the Impact of Circulation Patterns in Houston, TX, Journal of Geophysical Research: Atmospheres, 124(23), 13457–  
874 13474., <https://doi.org/10.1029/2019jd031725>, 2019.

875 Caicedo, V., Rappenglueck, B., Cuchiara, G., Flynn, J., Ferrare, R., Scarino, A. J., Berkoff, T., Senff, C., Langford, A., and  
876 Lefer, B.: Bay Breeze and Sea Breeze Circulation Impacts on the Planetary Boundary Layer and Air Quality from an  
877 Observed and Modeled Discover-AQ Texas Case Study, Journal of Geophysical Research: Atmospheres, 124(13),  
878 7359-7378, <https://doi.org/10.1029/2019jd030523>, 2019.

879 ~~Charrad, M., Ghazzali, N., Boiteau, V., and Niknafs, A.: NBCLUST: An R package for Determining the Relevant Number of~~  
880 ~~Clusters in a Data Set, Journal of Statistical Software, 61,(6), <https://doi.org/10.18637/jss.v061.i06>, 2014.~~

881 Christiansen, B.: Atmospheric Circulation Regimes: Can Cluster Analysis Provide the Number?, Journal of Climate, 20(10),  
882 2229–2250., <https://doi.org/10.1175/jcli4107.1>, 2007.

883 Coggon, M. M., Gkatzelis, G. I., McDonald, B. C., Gilman, J. B., Schwantes, R. H., Abuhassan, N., Aikin, K. C., Arend, M.  
884 F., Berkoff, T. A., and Brown, S. S.: Volatile chemical product emissions enhance ozone and modulate urban  
885 chemistry, Proceedings of the National Academy of Sciences, 118,32, National Academy of Sciences,  
886 <https://doi.org/10.1073/pnas.2026653118>, 2021.

887 Couillard, M. H., Schwab, M. J., Schwab, J. J., Lu, C. H., Joseph, E., Stutsrim, B., Shrestha, B., Zhang, J., Knepp, T. N., and  
888 Gronoff, G. P., Vertical Profiles of Ozone Concentrations in the Lower Troposphere Downwind of New York City  
889 during LISTOS 2018-2019, Journal of Geophysical Research: Atmospheres, 126(23), e2021JD035108,  
890 <https://doi.org/10.1029/2021JD035108>, 2021.

891 Darby, L. S.: Cluster Analysis of Surface Winds in Houston, Texas, and the Impact of Wind Patterns on Ozone, Journal of  
892 Applied Meteorology, 44(12), 1788–1806., <https://doi.org/10.1175/jam2320.1>, 2005.

893 Davis, R. E., Normile, C. P., Sitka, L., Hondula, D. M., Knight, D. B., Gawtry, S. P., and Stenger, P. J.: A Comparison of  
894 Trajectory and Air Mass Approaches to Examine Ozone Variability, *Atmospheric Environment*, 44(1), 64–74.,  
895 <https://doi.org/10.1016/j.atmosenv.2009.09.038>, 2010.

896 De Young, R., Carrion, W., Ganoe, R., Pliutau, D., Gronoff, G., Berkoff, T., and Kuang, S.: Langley Mobile Ozone LIDAR:  
897 Ozone and Aerosol Atmospheric Profiling for Air Quality Research, *Applied Optics*, 56(3), 721,  
898 <https://doi.org/10.1364/ao.56.000721>, 2017.

899 Dreesen, J., Orozco, D., Boyle, J., Szymborski, J., Lee, P., Flores, A., and Sakai, R. K.: Observed Ozone over the Chesapeake  
900 Bay Land-Water Interface: The Hart-Miller Island Pilot Project, *Journal of the Air & Waste Management Association*,  
901 69, (11), 1312–1330, <https://doi.org/10.1080/10962247.2019.1668497>, 2019.

902 EPA NEI (National Emissions Inventory v1): Air Pollutant Emission Trends Data, available at:  
903 <http://www.epa.gov/ttn/chief/trends/index.html> last access: 23 June 2015.

904 Farris, B. M., Gronoff, G. P., Carrion, W., Knepp, T., Pippin, M., and Berkoff, T. A.: Demonstration of an off-Axis Parabolic  
905 Receiver for near-Range Retrieval of Lidar Ozone Profiles, *Atmospheric Measurement Techniques*, 12(1), 363–370,  
906 <https://doi.org/10.5194/amt-12-363-2019>, 2019.

907 Gelaro, R., Gelaro, R., McCarty, W., Suárez, M. J., Todling, R., Molod, A., Takacs, L., Randles, C. A., Darmenov, A.,  
908 Bosilovich, M. G. Reichle, R., Wargan, K., Coy, L., Cullather, R., Draper, C., Akella, S., Buchard, V., Conaty, A., da  
909 Silva, A. M., Gu, W., Kim, G.-K., Koster, R., Lucchesi, R., Merkova, D., Nielsen, J. E., Partyka, G., Pawson, S., Putman,  
910 W., Rienecker, M., Schubert, S. D., Sienkiewicz, M., and Zhao, B.: The Modern-Era Retrospective Analysis for Research  
911 and Applications, Version 2 (Merra-2), *Journal of Climate*, 30(14), 5419–5454., <https://doi.org/10.1175/jcli-d-16-0758.1>,  
912 2017.

913 Gronoff, G., Robinson, J., Berkoff, T., Swap, R., Farris, B., Schroeder, J., Halliday, H.S., Knepp, T., Spinei, E., Carrion,  
914 W., Adcock, E.E., Johns, Z., Allen, D., Pippin, M.: A Method for Quantifying near Range Point Source Induced O<sub>3</sub>  
915 Titration Events Using Co-Located Lidar and Pandora Measurements, *Atmospheric Environment*, 204, 43–52,  
916 <https://doi.org/10.1016/j.atmosenv.2019.01.052>, 2019

917 Gronoff, G., Berkoff, T., Knowland, K.E., Lei, L., Shook, M., Fabbri, B., Carrion, W., Langford, A. O.: Case study of  
918 stratospheric Intrusion above Hampton, Virginia: lidar-observation and modeling analysis, *Atmospheric Environment*,  
919 259,118498, 1352-2310, <https://doi.org/10.1016/j.atmosenv.2021.118498>, 2021.

920 Han, J. and Kamber, M.: *Data mining: concepts and techniques*, San Francisco: Morgan Kaufmann Publishers, 2001.

921 Holmes, C. D., Bertram, T. H., Confer, K. L., Graham, K. A., Ronan, A. C., Wirks, C. K., and Shah, V.: The Role of Clouds  
922 in the Tropospheric NO<sub>x</sub> Cycle: A New Modeling Approach for Cloud Chemistry and Its Global Implications, *Geophys.*  
923 *Res. Lett.*, 46, 4980–4990, <https://doi.org/10.1029/2019GL081990>, 2019.

924 Hu, L., Keller, C. A., Long, M. S., Sherwen, T., Auer, B., Da Silva, A., Nielsen, J. E., Pawson, S., Thompson, M. A., Trayanov,  
925 A. L., Travis, K. R., Grange, S. K., Evans, M. J., and Jacob, D. J.: Global simulation of tropospheric chemistry at 12.5 km

926 resolution: performance and evaluation of the GEOS-Chem chemical module (v10-1) within the NASA GEOS Earth  
927 system model (GEOS-5 ESM), *Geosci. Model Dev.*, 11, 4603–4620, <https://doi.org/10.5194/gmd-11-4603-2018>, 2018.

928 ~~Kaufman, L. and Rousseeuw, P.: Finding groups in data: An introduction to cluster analysis, New York, Wiley, 1990.~~

929 Keller, C.A., Knowland, K.E., Duncan, B.N., Liu, J., Anderson, D.C., Das, S., Lucchesi, R.A., Lundgren, E.W., Nicely, J.M.,  
930 Nielsen, E., Ott, L.E., Saunders, E., Strode, S.A., Wales, P.A., Jacob, D.J., and Pawson, S.: Description of the NASA  
931 Geos Composition Forecast Modeling System GEOS-CF v1.0, *Journal of Advances in Modeling Earth Systems*, 13(4),  
932 <https://doi.org/10.1029/2020ms002413>, 2021.

933 Knowland, K.E., Keller, C.A., Lucchesi, R.: File specification for GEOS-CF products, GMAO office note No. 17 (version  
934 1.0). available from: [https://gmao.gsfc.nasa.gov/pubs/office\\_notes.php](https://gmao.gsfc.nasa.gov/pubs/office_notes.php), 32, 2019.

935 Knowland, K. E., Keller, C. A., Wales, P. A., Wargan, K., Coy, L., Johnson, M. S., Liu, J., Lucchesi, R. A., Eastham, S. D.,  
936 Fleming, E. L., Liang, Q., Leblanc, T., Livesey, N. J., Walker, K. A., Ott, L. E., and Pawson, S.: NASA GEOS  
937 Composition Forecast Modeling System GEOS-CF v1.0: Stratospheric Composition, 14(6), e2021MS002852,  
938 <https://doi.org/10.1002/essoar.10508148.1>, 2021.

939 Lawson, R. G., and Jurs, P. C.: New Index for Clustering Tendency and Its Application to Chemical Problems, *Journal of*  
940 *Chemical Information and Computer Sciences*, 30(1), 36–41., <https://doi.org/10.1021/ci00065a010>, 1990.

941 Leblanc, T., Brewer, M. A., Wang, P. S., Granados-Muñoz, M. J., Strawbridge, K. B., Travis, M., Firanski, B., Sullivan, J. T.,  
942 McGee, T. J., Sumnicht, G. K., Twigg, L. W., Berkoff, T. A., Carrion, W., Gronoff, G., Aknan, A., Chen, G., Alvarez,  
943 R. J., Langford, A. O., Senff, C. J., Kirgis, G., Johnson, M. S., Kuang, S., and Newchurch, M. J.: Validation of the TOLNet  
944 lidars: the Southern California Ozone Observation Project (SCOOP), *Atmos. Meas. Tech.*, 11, 6137–6162,  
945 <https://doi.org/10.5194/amt-11-6137-2018>, 2018.

946 Lei, L., Berkoff, T. A., Gronoff, G., Su, J., Nehrir, A. R., Wu, Y., Moshary, F., and Kuang, S.: Retrieval of UVB aerosol  
947 extinction profiles from the ground-based Langley Mobile Ozone Lidar (LMOL) system, *Atmos. Meas. Tech.*, 15, 2465–  
948 2478, <https://doi.org/10.5194/amt-15-2465-2022>, 2022.

949 Li, W., Wang, Y., Bernier, C., and Estes, M.: Identification of Sea Breeze Recirculation and Its Effects on Ozone in Houston,  
950 TX, during Discover-Aq 2013, *Journal of Geophysical Research: Atmospheres*, 125(22),  
951 <https://doi.org/10.1029/2020jd033165>, 2020.

952 Little, R. J., A., and Rubin, D., B.: *Statistical Analysis with Missing Data*. Second ed., Wiley, 1987.

953 Loughner, C. P., Tzortziou, M., Follette-Cook, M., Pickering, K. E., Goldberg, D., Satam, C., Weinheimer, A., Crawford, J.  
954 H., Knapp, D. J., Montzka, D. D., Diskin, G. S., and Dickerson, R. R.: Impact of Bay-Breeze Circulations on Surface Air  
955 Quality and Boundary Layer Export. *Journal of Applied Meteorology and Climatology*, 53, 7, 1697–1713.,  
956 <https://doi.org/10.1175/jamc-d-13-0323.1>, 2014.

957 Mao, J., Zhao, T., Keller, C. A., Wang, X., McFarland, P. J., Jenkins, J. M., and Brune, W. H.: Global Impact of Lightning-  
958 Produced Oxidants, *Geophys. Res. Lett.*, 48, <https://doi.org/10.1029/2021GL095740>, 2021.

959 McDuffie, E. E., Smith, S. J., O'Rourke, P., Tibrewal, K., Venkataraman, C., Marais, E. A., Zheng, B., Crippa, M., Brauer,  
960 M., and Martin, R. V.: A global anthropogenic emission inventory of atmospheric pollutants from sector- and fuel-specific  
961 sources (1970–2017): an application of the Community Emissions Data System (CEDS), *Earth Syst. Sci. Data*, 12, 3413–  
962 3442, <https://doi.org/10.5194/essd-12-3413-2020>, 2020.

963 Neuman, J. A., Trainer, M. Aikin, K., Brioude, J. Brown, S., de Gouw, J., Dube, W., Flynn, J., Graus, M., Holloway, J., Lefer,  
964 B., Nedelec P., Nowak, J., Parrish, D., Pollack, I., Roberts, J., Ryerson, T., Smit, H., Thouret, V., and Wagner, N.:  
965 Observations of Ozone Transport from the Free Troposphere to the Los Angeles Basin, *Journal of Geophysical Research:*  
966 *Atmospheres*, 117, 21, <https://doi.org/10.1029/2011jd016919>, 2012.

967 Orbe, C., Oman, L. D., Strahan, S. E., Waugh, D. W., Pawson, S., Takacs, L. L., and Molod, A. M.: Large-scale atmospheric  
968 transport in GEOS replay simulations, *J. Adv. Model. Earth Syst.*, 9, 2545–2560, <https://doi.org/10.1002/2017MS001053>,  
969 2017.

970 Ring, A. M., Canty, T. P., Anderson, D. C., Vinciguerra, T. P., He, H., Goldberg, D. L., Ehrman, S. H., Dickerson, R. R., and  
971 Salawitch, R. J.: Evaluating commercial marine emissions and their role in air quality policy using observations and the  
972 CMAQ model, *Atmospheric Environment*, 173, 96-107, <https://doi.org/10.1016/j.atmosenv.2017.10.037>, 2018.

973 Stauffer R.M., Thompson A.M., and Witte J.C.: Characterizing Global Ozone Profile Variability from Surface to the  
974 UT/LS with a Clustering Technique and MERRA-2 Reanalysis, *J Geophys Res Atmos.* 123(11):6213-6229.  
975 <https://doi.org/10.1029/2018JD028465>, 2018.

976 Strode, S. A., Ziemke, J.R., Oman, L. D., Lamsal, L. N., Olsen, M. A., and Liu, J.: Global changes in the diurnal cycle of  
977 surface ozone, *Atmospheric Environment*, 199, 323-333, <https://doi.org/10.1016/j.atmosenv.2018.11.028>, 2019.

978 Sullivan, J. T., McGee, T. J., Leblanc, T., Sumnicht, G. K., and Twigg, L. W.: Optimization of the GSFC TROPOZ DIAL  
979 retrieval using synthetic lidar returns and ozonesondes – Part 1: Algorithm validation, *Atmos. Meas. Tech.*, 8, 4133–  
980 4143, <https://doi.org/10.5194/amt-8-4133-2015>, 2015.

981 Sullivan, J.T., McGee, T.J., DeYoung, R., Twigg, L.W., Sumnicht, G.K., Pliutau, D., Knepp, T., and Carrion, W.: Results  
982 from the NASA GSFC and LaRC Ozone Lidar intercomparison: new mobile tools for atmospheric research, *J. Atmos.*  
983 *Ocean. Technol.*, 32 (10), 1779-1795, <https://doi.org/10.1175/JTECH-D-14-00193.1>, 2015.

984 Thompson, A. M., Stauffer, R. M., Miller, S. K., Martins, D. K., Joseph, E., Weinheimer, A. J., and Diskin, G. S.: Ozone  
985 profiles in the Baltimore-Washington region (2006-2011): satellite comparisons and DISCOVER-AQ observations, *J*  
986 *Atmos Chem.*, 72(3-4), 393-422. <https://doi.org/10.1007/s10874-014-9283-z>, 2015.

987 Torgo, L.: *Data Mining with R*, Chapman & Hall/CRC Data Mining and Knowledge Discovery Series,  
988 <https://doi.org/10.1201/b10328>, 2010.

989 Wang, L., Newchurch, M. J., Alvarez, R. J., Berkoff, T. A., Brown, S. S., Carrion, W., De Young, R. J., Johnson, B. J., Ganoe,  
990 R., Gronoff, G., Kirgis, G., Kuang, S., Langford, A. O., Leblanc, T., McDuffie, E. E., McGee, T. J., Pliutau, D., Senff,  
991 C. J., Sullivan, J. T., Sumnicht, G., Twigg, L. W., and Weinheimer, A. J.: Quantifying TOLNet Ozone Lidar Accuracy

992 during the 2014 DISCOVER-AQ and FRAPPÉ Campaigns. *Atmos Meas Tech*, 10(10), 3865-3876,  
993 <http://doi.org/10.5194/amt-10-3865-2017>. 2017.

994 Wang, X., Jacob, D. J., Downs, W., Zhai, S., Zhu, L., Shah, V., Holmes, C. D., Sherwen, T., Alexander, B., Evans, M. J.,  
995 Eastham, S. D., Neuman, J. A., Veres, P. R., Koenig, T. K., Volkamer, R., Huey, L. G., Bannan, T. J., Percival, C. J.,  
996 Lee, B. H., and Thornton, J. A.: Global tropospheric halogen (Cl, Br, I) chemistry and its impact on oxidants, *Atmospheric*  
997 *Chem. Phys.*, 21, 13973–13996, <https://doi.org/10.5194/acp-21-13973-2021>, 2021.

998 Wu, Y., Nehrir, A. R., Ren, X., Dickerson, R. R., Huang, J., Stratton, P. R., Gronoff, G., Kooi, S. A., Collins, J. E., and  
999 Berkoff, T. A.: Synergistic aircraft and ground observations of transported wildfire smoke and its impact on air quality  
.000 in New York City during the summer 2018 LISTOS campaign, *Science of The Total Environment*, 773,145030,  
.001 <https://doi.org/10.1016/j.scitotenv.2021.145030>, 2021.